J. Fluid Mech. (1992), *vol.* 243, *pp.* 261–296
Printed in Great Britain

Breakdown regimes of inertia waves in a precessing cylinder

By RICHARD MANASSEH†
Department of Applied Mathematics and Theoretical Physics, University of Cambridge, Silver Street, Cambridge CB3 9EW, UK

(Received 8 October 1991)

A series of experimental studies have been made of the fluid behaviour in a completely filled, precessing, right circular cylinder. The tank was spun about its axis of symmetry and subjected to a forced precession at various excitation frequencies ω, nutation angles θ and at various Ekman numbers. This forcing excites a subset of the modes, called *inertia waves*, that are made possible by the Coriolis force that arises in a spinning environment. In these experiments, the fluid flow breakdown phenomena are investigated. Here the fluid, when forced near a resonant frequency, exhibits a transition to disordered or turbulent flow. This paper presents a categorization of some of the breakdown regimes, of which the 'resonant collapses' (McEwan 1970) are the most catastrophic members.

The studies reported in this paper used entirely visual observations and measurements. The experimental observations employed a visualization technique that gave no information on fluid velocities, but provided an excellent picture of the flow structure. Quantitative data were extracted in the form of the time for the breakdown to occur. The breakdown phenomena, while readily produced over a large region of parameter space, are complex and varied. The observations show that our system is extraordinarily rich, exhibiting, for example, recurrent breakdowns which may be explained in terms of chaotic intermittency. A detailed description of some of the different *breakdown regimes* indicates that no single model will explain the behaviour throughout parameter space. This research is motivated by the instability problems of spinning spacecraft containing liquid fuels.

1. Introduction

If a rotating fluid is subjected to forcing that is time-harmonic and of constant amplitude, with the excitation frequency ω_1 less than twice the basic spin rate Ω, a class of waves is possible. These waves, often called *inertia waves*, are only possible in a rotating environment; it is the Coriolis force that provides the 'restoring force' that enables them to exist.

Several theoretical and experimental studies have been made of the problem of inviscid forced oscillations in a completely filled cylindrical container. Right circular cylindrical boundary conditions permit a separable solution for the flow in terms of eigenmodes. The eigenfrequencies for the fluid normal modes were first produced by Lord Kelvin (1880). Further theoretical studies of inertial oscillations in a right circular cylinder include those of Wood (1965, 1966), Baines (1967), Gans (1970) and Thompson (1970).

† Current affiliation: School of Mathematics, Oceanography Group, University of New South Wales, PO Box 1, Kensington, NSW 2033, Australia.

The resonant frequencies predicted by linear inviscid theory have been shown to be quite accurate in a number of experiments. Fultz (1959) got excellent agreement with the theoretical resonant frequencies for the axially symmetric modes. His forcing regime consisted of a disc vibrating along the axis of a spinning cylinder. McEwan (1970) again found linear inviscid theory to be accurate, in predicting the aspect ratios for resonance of the fluid in a spinning cylinder. Forcing was by means of an top end-cap rotating independently at an angle to the bottom of the cylinder. The excitation frequency was effectively varied by changing the cylinder height. The modes could be clearly identified through flow visualization.

However, experimental studies have shown that very complicated behaviour can arise, in both right circular cylinders and in other geometries. In some cases, instabilities in the forced fluid have degenerated into turbulence. Johnson (1967) first published an observation of breakdowns of inertia waves. At the same time Malkus (1968) was observing breakdowns in a precessing spheroid. Malkus (1968), McEwan (1970), Gans (1970), Scott (1975), Whiting (1981) and Stergiopoulos & Aldridge (1982) all reported instabilities or turbulence developing in experiments where contained inertia waves were forced.

McEwan (1970) first used the term *resonant collapse* in a description of his detailed experimental work. After resonant forced flow had been established for some time, instabilities appeared and the motion degenerated into disorder and fine-scale turbulence. Timescales for instabilities to appear were of orders 10 to 100 revolutions. McEwan found the timescales for the collapse were quite consistent for the same values of the forcing parameters. The occurrence of the collapse was predictable and collapses occurred when a wide variety of fluid modes were forced at resonance. Furthermore, McEwan noted that the disorder after the collapse waxed and waned and that in some cases the modal waveform 're-emerged periodically'. Later, McEwan (1971) was to speculate that the 'resonant collapse' of inertia wave modes was caused by nonlinear interactions of triads of waves. This triad mechanism successfully modelled the degeneration of internal waves in a stratified fluid (McEwan, Mander & Smith 1972; McEwan 1983).

Recently, similar phenomena have been observed in the context of studies of elliptical flow instabilities. When the basic streamlines are elliptical, it can be shown (Waleffe 1988) that there is a most unstable inertia wave mode. Experiments (Malkus 1989) have shown that 'resonant collapse' type breakdowns in these systems can occur. Malkus (1989) reported on elliptical flow instabilities, observed in experiments using a cylinder with flexible sidewalls. Since the aspect ratio of the cylinder is selected to be close to a resonance, a mode forms and undergoes a breakdown that is qualitatively very similar to the Type A and D breakdowns described in §4 below. Calculations of *bounded* elliptical flow instabilities had been done previously by Gledzer and colleagues, although these were only reported informally in Gledzer, Dolzhanskii & Oboukhov (1989) which described experiments where the most unstable modes were observed in a cylinder with elliptical cross-section after rotation was abruptly stopped. The fluid was thus forced to follow elliptical streamlines. Previously, in Gledzer *et al.* (1974) a similar experiment had been performed with an ellipsoidal cavity.

The linear inviscid solution outlined in §2 will lead one to expect the fluid behaviour to consist of a set of ordered inertia wave modes. The experimental observations were set up with the following two aims: (i) to test the predictions of linear inviscid theory of the locations of low-order eigenfrequencies in the ω-spectrum; (ii) to identify and characterize the general behaviour of the fluid over a

wide range of parameters. The experimental apparatus used in this work is described in §3. Also in that section are details of the procedure and techniques used in the experiments. The experimental observations, and some discussion of the interpretation of the resulting images of the flow, are presented in §4.

2. Linear inviscid theory

Referring to figure 1, consider a general fluid-filled container spinning about an axis through its centroid and precessing about a second axis through its centroid. Assume the centroid is not accelerating in inertial space, and the angle between the two axes is not varying with time. In rotating fluid dynamics problems one typically chooses the basic rotation period of the fluid relative to inertial space as the timescale; in our problem this is $\Omega^{-1} = |(\omega_1 \hat{\boldsymbol{k}} + \omega_2 \hat{\boldsymbol{K}})|^{-1}$, where the symbols are as defined on figure 1. Here, however, we shall choose the timescale to be ω_1^{-1}. In making this choice, we are anticipating observing experiments from a frame of reference in which periods of ω_1^{-1} are easily counted to provide a timescale with which various events can be measured. In fact, in the experiments to be described later, ω_1^{-1} is the rotation period of the container relative to the observing cameras. The lengthscale L is equal to the container diameter. The cylinder length/diameter aspect ratio is h. We assume that the *nutation angle* θ between the two axes is small, and assuming that the velocity scale $U = O(\omega_1 L\theta)$ allows linearization of the problem. The dimensional pressure is $\rho\omega_1 ULp$ where p is the dynamic pressure in excess of the centrifugal pressure, which plays no dynamical role in this problem. The non-dimensional excitation frequency, ω, is defined as twice the ratio of the basic rotation rate $\boldsymbol{\Omega}$ to the frequency of the variation of the overall angular velocity vector in container coordinates, ω_1, giving to first order in θ

$$w = 2(1 + w_2/w_1).$$

Adopt cylindrical polar coordinates (r, ϕ, z) fixed in the container. The origin of the tank-fixed coordinates is the container centroid. The coordinates are referenced to a unit vector triad $(\hat{\boldsymbol{\rho}}, \hat{\boldsymbol{\Phi}}, \hat{\boldsymbol{k}})$. The incompressible, inviscid linearized fluid equation of motion relative to axes *fixed in the container* is

$$\frac{\partial \boldsymbol{u}}{\partial t} + \omega \hat{\boldsymbol{k}} \times \boldsymbol{u} + \nabla p = -(\omega - 2)\,(r\cos(\phi + t))\,\hat{\boldsymbol{k}}, \tag{1a}$$

together with incompressibility,

$$\nabla \cdot \boldsymbol{u} = 0. \tag{1b}$$

Equation (1*a*) is the form of the momentum equation appropriate to our problem; steps in its derivation are outlined in Wood (1966). Its homogeneous form expresses the balance between inertia, Coriolis and pressure gradient forces. The inhomogeneous term on the right-hand side comes from the variation of the overall angular velocity vector with time, due to the precession imposed on the container. This is the forcing applied to the system. The boundary condition is

$$\boldsymbol{u} \cdot \hat{\boldsymbol{n}} = 0, \tag{1c}$$

where $\hat{\boldsymbol{n}}$ is the unit normal vector to the container surface. This allows a free-slip condition at the container wall consistent with our assumption of an inviscid flow, in

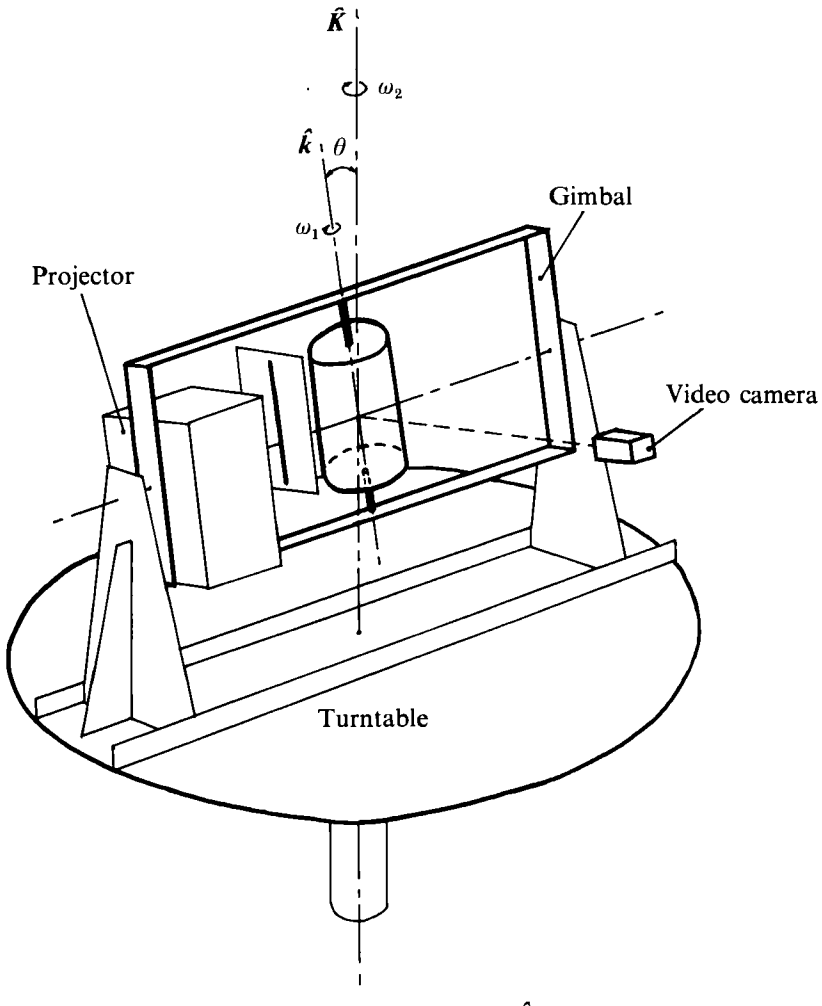

FIGURE 1. Schematic diagram of the apparatus. The unit vector $\hat{k}$ is fixed in the spinning tank; the unit vector $\hat{K}$ is fixed in the turntable. The video camera is fixed in the turntable frame; its line of sight is normal to $\hat{k}$.

k	l	ω_n	λ_n	k	l	ω_n	λ_n
1	1	2.64298	2.88221	4	1	1.12769	2.45622
1	2	5.27757	6.10489	4	2	1.55603	5.61787
1	3	7.93621	9.27678	4	3	2.11440	8.77909
2	1	1.48403	2.58361	5	1	1.08229	2.43833
2	2	2.65374	5.79180	5	2	1.37830	5.58728
2	3	3.93395	8.96470	5	3	1.78975	8.74335
3	1	1.22370	2.49274	6	1	1.05736	2.42833
3	2	1.89134	5.67380	6	2	1.27306	5.56886
3	3	2.69398	8.84105	6	3	1.58812	8.72081

TABLE 1. Resonant excitation frequencies ω_n and radial wavenumbers λ_n for a precessionally forced cylinder, $h = \frac{4}{3}$

which the Ekman number, defined as $E \equiv \nu/(\omega_1 L^2)$, has been assumed to be negligibly small.

To find the set of wave modes in a cylindrical tank, one seeks a complementary function to (1*a*) satisfying the inviscid boundary conditions. Assuming a separable solution of form

$$\boldsymbol{u} = \sum_{n=1}^{\infty} \boldsymbol{U}_n \mathrm{e}^{\mathrm{i}t},$$

$$p = \sum_{n=1}^{\infty} Q_n(r, \phi, z)\, \mathrm{e}^{\mathrm{i}t},$$

and eliminating the velocity components with the aid of the continuity equation, we get Poincaré's equation,

$$\frac{1}{r}\frac{\partial}{\partial r}\left(r\frac{\partial Q_n}{\partial r}\right)+\frac{1}{r^2}\frac{\partial^2 Q_n}{\partial \phi^2}+(1-\omega^2)\frac{\partial^2 Q_n}{\partial z^2} = 0, \tag{2a}$$

a hyperbolic p.d.e. for $|\omega| > 1$. The associated boundary condition is

$$\boldsymbol{U}_n \cdot \hat{\boldsymbol{n}} = 0. \tag{2b}$$

In general (2*a*) admits a set of plane-wave solutions, which are usually referred to as *inertia waves*. Although the full problem (2) is ill-posed, it is possible to find an analytic description of the flow in this case because of the particular geometry of a right circular cylinder.

For brevity the index n will be used to indicate a unique combination of the spatial wavenumbers k, λ and m. The integer k is the axial wavenumber and the integer m is the azimuthal wavenumber. As the radial wavenumber λ is non-integer, it is convenient to use an integer index l to count the number of half-cycles in the radial direction. The wavenumber vector is then $\{k, l, m\}^{\mathrm{T}}$. Strictly, it should be noted that waves with the same (k, l, m) but negative phase speeds have a different spatial structure in this problem, and hence a fourth index should be used to specify the direction of phase propagation. However, in these experiments, only waves with a positive phase speed are forced.

A solution to (2) by separation of variables is

$$Q_n = J_m(2\lambda_n r)\cos\left(2(\omega^2-1)^{-\frac{1}{2}}\lambda_n[z+\tfrac{1}{2}h]\right)\mathrm{e}^{\mathrm{i}m\phi},$$

where J_m is the Bessel function of the first kind, order m. A solution to Poincaré's equation of this kind was first found by Kelvin (1880) and is quoted in Greenspan (1968).

For precessional forcing, which requires $m = 1$, the radial wavenumbers are given by the roots of

$$\lambda J_1'(\lambda)+\omega J_1(\lambda) = 0, \tag{3}$$

in order to satisfy the radial boundary condition. In order to satisfy the axial boundary condition with integer k,

$$\omega^2 = 1+\left(\frac{2\lambda_{kl1}h}{k\pi}\right)^2, \tag{4}$$

where λ_{kl1} is the lth root of (3). Resonant excitation frequencies are thus values of ω satisfying (3) and (4).

The real velocity field corresponding to a single mode is given by

$$\boldsymbol{u}_n = \frac{(1-\frac{1}{2}\omega)f_n}{1-\omega/\omega_n}\Bigg\{-\frac{1}{1-\omega_n^2}\left[\frac{\mathrm{d}J_1(2\lambda_n r)}{\mathrm{d}r}+\omega_n\frac{1}{r}J_1(2\lambda_n r)\right]\cos\left[k\pi(z/h+\tfrac{1}{2})\right]\sin(\phi+t)$$

$$\frac{-1}{1-\omega_n^2}\left[\omega_n\frac{\mathrm{d}J_1(2\lambda_n r)}{\mathrm{d}r}+\frac{1}{r}J_1(2\lambda_n r)\right]\cos\left[k\pi(z/h+\tfrac{1}{2})\right]\cos(\phi+t)$$

$$\frac{k\pi}{h}J_1(2\lambda_n r)\sin\left[k\pi(z/h+\tfrac{1}{2})\right]\sin(\phi+t)\Bigg\}, \tag{5}$$

where (Kudlick 1966) f_n is calculated by taking the projection of the forcing function onto the spatial structure of the nth mode and ω_n is a solution to (4). Further details of this calculation are in Manasseh (1991).

Some of the lower-order resonant excitation frequencies are given in table 1 for the cylinder length/diameter ratio h of the experiment in this study.

The spatial structure of the forced solution rotates in the tank coordinates with frequency $-\omega_1$. It is stationary relative to the forcing function, which is fixed in the *precessing* frame of reference. In the experimental apparatus shown in figure 1, this precessing frame is the turntable on which the cameras are fixed. The video camera in figure 1 is fixed in this precessing frame of reference, and so should see a stationary spatial structure corresponding to the forced solution. Similarly, a photographic camera is also fixed on the turntable, on the opposite side of the tank to the video camera. In effect, the cameras are 'following' the travelling wave pattern around the tank.

In principle all the linear inviscid modes could be excited, up to the order where the wavelength is comparable to the boundary-layer thickness. However, the modes that can be precessionally forced have $m = 1$, as noted above. Furthermore, the forcing function, $-(\omega-2)(r\cos(\phi+t))\,\hat{\boldsymbol{k}}$, is even in z, so the modes upon which it will project must have a vertical velocity that is also even in z, requiring, from (5), an odd axial wavenumber k. In practice, the dense spacing of the resonant frequencies and the complex behaviour described in §4, prevent direct observation of all such modes. In addition, the factor $(1-\frac{1}{2}\omega)$ in (5) means that those modes with ω close to 2.0 will be forced with only a small amplitude. The experimental apparatus could force the system with an positive ω value of up to 2.8. Thus in the following descriptions *low-order* will be taken to mean ω not close to 2.0 and less than 2.8, and with wavenumber vector magnitudes less than about 7. In addition *expressed* modes will be taken to mean low-order modes with $m = 1$ and k odd, and the term *easily forced* will be used to indicate that the magnitude of the factor $((1-\frac{1}{2}\omega)f_n)/(1-\omega/\omega_n)$ in equation (5) is large.

3. Apparatus and experimental procedure

3.1. *Apparatus*

Full details of the experimental apparatus and procedure are in Manasseh (1991). The apparatus is sketched in figure 1. The Perspex tank is of internal diameter 90 mm and internal height 120 mm. For the experiments reported here the tank was completely filled. The fluid used was distilled water. The tank spins in a gimbal frame which is in turn mounted on a turntable. Thus ω_1 is the spin rate of the tank in the gimbal frame and the precession rate ω_2 is the turntable speed. The nutation angle

θ can be varied by tilting the gimbal frame from the vertical. The tank spin axis is precessed at constant θ. This nutation angle is preset at a desired value and precession is initiated by an impulsive tilt of the gimbal frame to the preset value.

Flow inside the tank is illuminated by a plane sheet of white light and is viewed by cameras with a line of sight normal to this plane. Simultaneous still photography is also possible. The flow field inside the tank is visualized by the introduction of pearlescent flakes. It can be assumed (Savaş 1985) that these highly reflective flakes are aligned at a particular inclination to the velocity gradient in the fluid. Use of pearlescence should be regarded as an essentially qualitative technique, which gives a picture of the structure of the flow, but no information about the magnitudes of strain or velocity. The operating tank spin rate ω_1 was initially chosen to ensure that the Ekman number of the flow (defined as $E = \nu/(\omega_1 L^2)$) remained small of order 10^{-5}, without having to run the apparatus at dangerously high speeds. Thus it was expected that the inviscid interior model described in §2 would remain valid for these experiments.

3.2. *Experimental procedure*

To try to identify the modes as reported in §4.2, the following procedure was adopted: (i) The nutation angle θ was held fixed at 5°; (ii) ω_1 was set to an optimum value determined from tests; (iii) $|\omega_2|$ was increased in steps of 0.06 rad s^{-1} up to the maximum value, video recordings being made at each stage.

In most experiments the flow was observed to break down. Times from the commencement of forcing to the occurrence of the various breakdown phenomena (described in §4) were recorded. After experience had been gained in initial experiments, timings were made during experimentation by observations of the video images in real time. The times recorded here were times t_c scaled in revolutions of the tank relative to the cameras. A decision as to exactly when the breakdown has occurred is obviously subjective; in general this was defined as when the flow had reached its most turbulent or disordered stage. In §4, it is noted that different modes undergo different forms of breakdown; hence the precise definition of breakdown will depend on the mode being observed. The breakdown time measurements should therefore not be used for direct quantitative comparisons between the modes.

The procedure for recording breakdown times was as follows: (i) With $\omega_1 = \omega_2 = 0$ the desired nutation angle θ is preset. (ii) $|\omega_2|$ is increased to the desired value. (iii) ω_1 is increased smoothly by microcomputer control to the optimum operating value. (iv) Wait with $\theta = 0$ while the fluid spins up to solid-body rotation. The theoretical spinup time is calculated as $L((\omega_1+\omega_2)^{-\frac{1}{2}}\nu^{-\frac{1}{2}})$, where ν is the kinematic viscosity, and provides a guide to the minimum time to wait. Visualizations of the fluid during spinup also provide a guide as to the extent of the spinup process. (v) The gimbal tilts smoothly to the present angle. (vi) When the breakdown time is judged to have elapsed the time is recorded. Timing of subsequent secondary breakdowns is possible, as is the record of a 'no breakdown', which indicates that the flow did not break down according to one of the regimes described in §4. The 'no breakdown' record, however, includes the possibility of some weak instabilities occurring over long timescales. (vii) ω_1 and $|\omega_2|$ are decreased to zero. The spindown process generates turbulence due to centrifugal instabilities. This behaviour is exploited to ensure that any structure remaining in the flow is destroyed before the next run.

4. Experimental observations

4.1. *Initial state*

Before the impulsive start to precession the pearlescent image consists of a luminous zone surrounding the tank axis and a thin black core on the axis itself. In general the black core is particularly well defined. Figure 2 shows this state, before the commencement of forcing of the (1, 1, 1)-mode. Here $\theta = 0$ but ω at 2.643 is as close to the (1, 1, 1)-resonance as the accuracy of the equipment would permit. The *bright column* is defined to be the luminous zone near the tank centre, and the thin black core at the centreline of that zone. The presence of this bright column implies some strain in the fluid (Savaş 1985). This bright column is the remnant of a luminous zone that could be seen shrinking onto the tank axis during the spinup process. Evidently, therefore, the fluid in this column is not in uniform solid-body rotation, despite its stable persistence after many theoretical spinup times had elapsed. Tests had indicated that heat from the lighting was not responsible for the bright column. A series of experiments, to be reported in a later paper, was conducted using a dyeline technique. As part of these experiments, it was determined that the bright column present before the commencement of forcing did in fact correspond to a small departure from solid-body rotation, taking the form of a net circulation. This departure will be called the *anomaly drift*. The vorticity corresponding to the largest measured anomaly drift is of the order of 0.01 rad s^{-1}, and hence is of order 10^{-3} scaled relative to the basic spin ω_1 of about 10 rad s^{-1}. The minimum 'anomaly vorticity' is achievable after spinning up for about 3 h and is of order 10^{-4} in scaled form.

The cause of the anomaly drift observed is presumed to be the small oscillations in the basic spin rate ω_1 that could not be eliminated from the mechanical system. It is presumed that these oscillations, exacerbated by out-of-roundness irregularities in the tank wall, generate the departure from solid-body rotation. The dominant oscillation was itself at a frequency of about ω_1 and was about 0.5% of ω_1. The out-of-roundness irregularities were of order $10^{-2}L$. Further details are in Manasseh (1991). The actual mechanism for generating the anomaly drift may be akin to that described in Suess (1971), in which boundary-layer singularities are shown to require an axial shear layer in the interior flow.

This small departure of order 10^{-3} from solid-body rotation should not influence the linear mode development and the corresponding distribution of strain in the fluid. It is unlikely, therefore, that the most robust breakdown regimes reported here (Types A, B, D, E, F), are caused or influenced by this anomaly drift that is present before forcing begins. However, we cannot rule out the possibility that the more subtle breakdown regimes may be influenced by a weak net circulation.

Neither is the flow before the commencement of forcing immune from unsteady behaviour. If the system is left unforced, after a 'long' time in the order of a thousand revolutions unsteady motion generally becomes visible in the form of vertical luminous columns or striations apparently rotating with the tank. McEwan (1970) was likewise unable to eliminate irregular vertical striations in his experiment, that were present before the commencement of forcing.

It is possible that some of the long-timescale instabilities reported in the present paper are actually caused by thermal effects – heat coming from the incandescent light source. In general the temperature of the Perspex outer surface of the tank will rise by about 1 °C to an equilibrium of about 21 °C during a typical 20 min experimental run. If there were a radial temperature gradient in the tank, the

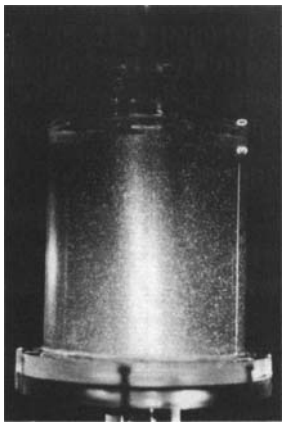

FIGURE 2. State before the commencement of forcing, $\theta = 0, \omega = 2.643$.

thermal wind equation would predict an axial gradient in a steady azimuthal circulation. If a temperature difference of 1 °C were applied across the tank radius, we should expect a difference in azimuthal circulation of about 4 mm s^{-1} between the tank top and bottom. However, as detailed in Manasseh (1991), the Perspex wall does not heat up by 1 °C instantaneously and it takes some time for this temperature difference to be conducted to a thin thermal boundary layer of about 1 mm thickness; typically this timescale is longer than that over which the most of breakdowns take place. In any case, in the parameter range of these experiments, once a transient impulse or a steady forcing is applied to the system, the resulting behaviour dominates any irregularities previously present.

4.2. *Behaviour following forcing*

4.2.1. *Identification of modes predicted by linear inviscid theory*

Noticeable transient motions could be generated by impulsively tilting the tank spin axis with $\omega_2 = 0$, through a large angle of about 10°. When viewed by the camera as in figure 1, the core and luminous column could be seen to rock from side to side and develop brief wavy modulations. The most obvious such modulation is the waveform of the fundamental mode (see §4.3). The apparent 'amplitude' of the half-angle of the rocking motion in the image is of the order of the tilt angle. As expected the motion dies away in the order of one spinup time, $E^{-\frac{1}{2}}/\omega_1$, which for the present set of parameters is about 30 s.

Three parameters are readily varied in this experimental system: the nutation angle θ, the forcing frequency ω, and, as detailed in §4.2.3, the Ekman number.

If ω is varied in small steps with θ fixed, as described in §3.2, the fluid will display different modes which are excited in turn. The modal response manifests itself as a bright wavy axial band. A typical example is shown in figure 3, where the system is being forced near the resonant ω for the (3, 1, 1)-mode. The line of sight of the cameras in figure 1 was in the plane of $\hat{\boldsymbol{k}}$ and $\hat{\boldsymbol{K}}$; the waveform appears normal to this line of sight. The waveform appears stationary when viewed from the precessing frame. As noted in §2 this is expected as the linear response is in phase or π out of phase with the forcing. Again as expected, $\frac{1}{2}k$ wavelengths fit in the tank height, as the linear solution (5) is proportional to $\cos(k\pi[z/h + \frac{1}{2}])$, for $-\frac{1}{2} < z/h < \frac{1}{2}$.

Recall from §3.1 that the pearlescence technique visualizes the structure of the

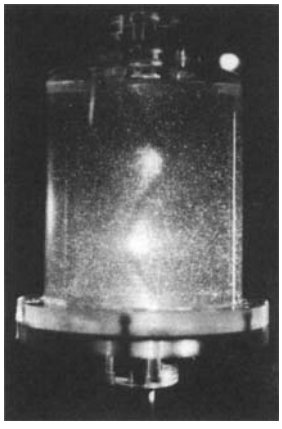

FIGURE 3. Typical modal response, $\theta = 1°, \omega = 1.260$.

flow and gives no information on the magnitudes of velocity or strain. The apparent 'amplitude' of the bright waveform, then, should be governed by the spatial structure of a mode near resonance, not its amplitude. However, the presence of the bright column before the commencement of forcing casts some doubt on this simple interpretation of the image. The tests noted in §4.1 indicated that the anomaly drift was only of order 10^{-3} scaled relative to the background vorticity due to the basic spin, and so should not significantly influence the development of the mode. However, if the magnitude of the flow due to the mode were as low in magnitude as the anomaly drift, might not the drift affect the visualization? One could, for instance, imagine a significant distortion of the fluid particle pathlines due to an inertia wave mode, and the corresponding strain distribution, if an anomaly drift of comparable magnitude were linearly superposed. This question was not resolved until further experiments were tried with the dyeline technique, to be reported in a later paper. As a consequence of this study, which permitted a direct comparison of the velocities of the anomaly drift and of the flow corresponding to inertia wave modes, it was found that in the great majority of cases, the anomaly drift is two orders of magnitude less than the flow corresponding to the inertia waves. Therefore we can assume in general that the pearlescent pattern represents only the structure of the flow.

The accuracy of the solution given in §2 was investigated by checking that the low-order resonant frequencies were located where predicted by linear inviscid theory, and by confirming that the axial wavenumber of the pattern visualized corresponded to that in equation (5). The resonances were located by visual inspection of the pearlescent pattern; ω was varied with θ fixed and the occurrence of any modal behaviour was noted at each ω. These qualitative investigations found eight out of 14 low-order resonant frequencies to be located where predicted in the ω-spectrum. The other six were either non-expressed, or were not seen for the reasons individually detailed below. Of these eight, six were expressed modes. As noted in §2, the non-expressed modes with even k cannot be directly forced, nevertheless two such modes were identified near their resonant frequencies. The reason for the appearance of the non-expressed modes is not clear.

In general, precise determination of the resonant frequency is obscured by the breakdown phenomena. Catastrophic breakdowns originally described by McEwan

(1970) as 'resonant collapses' (more precise definitions will be given in §§4.3 and 4.4 below) begin to occur for a fairly wide bandwidth on either side of the theoretical value. For example, for the (3, 1, 1)-mode, 'resonant collapses' can occur for $1.2 < \omega < 1.3$, the range depending on the nutation angle θ. From table 1 we see that the linear inviscid theory predicts a resonant frequency of 1.2237. In fact, to identify clearly a particular mode it was usually necessary to increase θ to a value which would result in a 'resonant collapse'. For these experiments the maximum forcing amplitude available, $\theta = 5°$, was used to ensure that as many modes as possible could be identified. Thus, in practice, checking the locations of resonant frequencies predicted by linear inviscid theory had to be done under conditions where the theory would ultimately break down.

Some low-order modes within the ω-range of the experimental equipment are: (1, 1, 1), (2, 1, 1), (2, 2, 1), (3, 1, 1), (3, 2, 1), (3, 3, 1), (4, 1, 1), (4, 2, 1), (4, 3, 1), (5, 1, 1), (5, 2, 1), (5, 3, 1), (6, 2, 1) and (6, 3, 1). The (2, 2, 1)- and (3, 3, 1)-modes are so close to the (1, 1, 1)-mode in the ω-spectrum that they could not be observed; any attempts to force them resulted in behaviour dominated by 'resonant collapse' of the (1, 1, 1)-mode. The (9, 3, 1)-mode was identified within the breakdown range of the (3, 1, 1)-mode. The (6, 2, 1)-mode, being non-expressed, was not identified. In addition to the (1, 1, 1)- and (3, 1, 1)-modes described in detail below, mode forms with the correct axial wavenumber, at predicted frequencies, were identified for the (3, 2, 1)-, (5, 2, 1)- and (5, 3, 1)-modes, as well as for the (4, 1, 1)- and (4, 2, 1)-modes, despite these last two being non-expressed. The behaviour noted near the (4, 1, 1)-mode resonant frequency was particularly complicated, with evidence of a secondary mode often present.

However, at the (2, 1, 1)-frequency the mode form visible seems to have approximately six axial half-wavelengths. The (5, 1, 1)-mode form was hard to identify unambiguously before its breakdown occurred. The (6, 3, 1)-mode was not observed. Clear characteristics can be observed along with the (4, 2, 1)-mode, with a conical half-angle of about 40°, the expected angle for the characteristics of the hyperbolic operator in (2).

Some form of flow instability or breakdown was observed within the timescale of several hundred revolutions of a typical experimental run, for all the modes identified above. However, particularly dramatic 'resonant collapses', involving transitions to turbulent flow or fine lengthscale disorder, were observed near the (1, 1, 1), (2, 1, 1), (3, 1, 1), (4, 1, 1), (5, 1, 1) and (5, 2, 1) resonant frequencies.

The 'low-order expressed modes' as defined in §2 are those modes that one might reasonably expect to see evidence of with the apparatus used in these experiments. In summary, patterns consistent with each of the low-order expressed modes were identified at approximately the frequencies predicted by linear inviscid theory. The one exception in these pearlescence observations was the (3, 3, 1)-mode; its resonance is so close to that of the (1, 1, 1)-mode that no evidence of it was observed. The degree of approximation in identifying the locations of the frequencies is governed by the breakdown behaviour near the resonant peak. If a general statement is to be made about the accuracy of the frequency locations, it is that the resonances appear to be within $\pm 10\%$ of the values predicted by linear inviscid theory.

4.2.2. *Breakdown of the modes*

The behaviour of the system, as revealed by these visualizations, is dominated by various breakdown phenomena. The flow, after displaying its modal waveform with the axial wavenumber as predicted by linear theory, becomes unstable and there is

a transition to turbulence or disorder. For strong forcing, say a tilt of $\theta = 3°$, the breakdown produces quite fine-grain turbulence, with an isotropic eddy size in the order of a tenth of the tank radius. Weak forcing produces flows best described as disordered rather than turbulent.

If ω is varied in small steps with θ fixed at, say, 5° (a 'large' angle in these experiments) the fluid displays the different low-order modes which are excited in turn, then are seen to undergo a breakdown. As ω passes out of range of a particular mode the fluid recovers an ordered flow until the range of the next mode is reached. If precession at a resonant frequency is started impulsively, as described in §3.2, the core and luminous column immediately begin to develop the modal structure. This structure will break down in the majority of cases, either with a catastrophic 'resonant collapse' or with some other forms of breakdown to be discussed shortly. It is interesting to note that the breakdown range of a particular mode is not centred on the resonant frequency of the mode.

When the (1, 1, 1)-mode is forced the breakdown is observed to occur for all but the smallest nutation angles, say θ of order $\frac{1}{10}°$. Apparently stable linear modeforms at larger θ of order 1° have been observed for some higher-order modes, for example the (5, 3, 1)- and (9, 3, 1)-modes. However, the experiments were not sufficiently exhaustive to rule out the possibility of instabilities affecting these modes on a long timescale of order several hundred revolutions. The (9, 3, 1)-mode may be dominated in certain regions of parameter space by the breakdown of the (3, 1, 1)-mode, which has a resonant frequency in the same narrow ω-bandwidth. In general, it appears that if a mode has a resonant ω such that it is low-order, it will exhibit some form of breakdown.

Different *breakdown regimes* have been identified. These are consistent and reproducible forms of flow behaviour leading up to and during the breakdown. Different regimes have been observed for each different mode, and furthermore different regimes can be observed when a particular mode is excited in different regions of parameter space. The behaviour after breakdown need not be completely disordered for all time. Even if forcing is maintained, the disorder may recover some modal structure. The disorder may wax and wane or, in many regions of parameter space, the flow after an initial breakdown becomes quite ordered and then undergoes further recurring breakdowns, the flow regaining some order in between breakdowns. Similar behaviour, described as 'periodic', was noted in McEwan (1970), and in an experiment reported by Scott (1975).

The occurrence of a breakdown does not depend on the way the precessional excitation is set up. Either an impulsive increase in θ from zero to a preset value, or a spinup of either ω_1 or ω_2 to a resonant combination, will cause a breakdown. It is possible that near the boundaries of the breakdown regimes, details of the breakdown process, or the type of breakdown regime observed, will be sensitive to initial conditions. However, there is not enough systematic data to be sure. Attempts were made to create a different type of breakdown by impulsively starting precession at different stages of the spinup process described in §3.2, for example a 20% change in the time before or after the luminous zone had reached its minimum diameter. However, for all such tests the qualitative behaviour remained essentially the same. The time from the commencement of forcing to the breakdown, when measured non-dimensionally in terms of the number of tank revolutions, is quite repeatable. This repeatability is despite variations in initial conditions. Following the measurement techniques described in §3.2, such timings were used to extract quantitative data on the influence of various parameters on the breakdown phenomena.

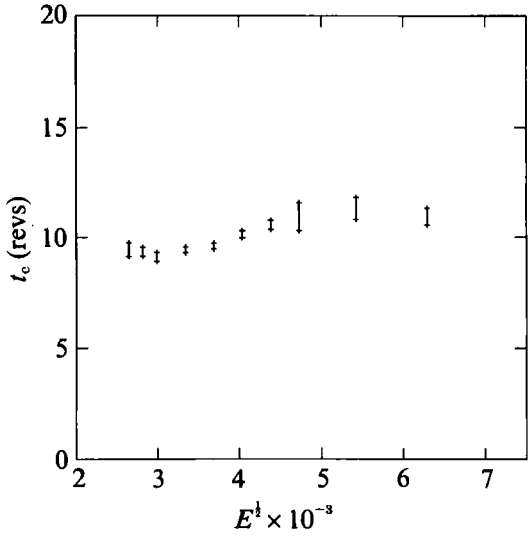

FIGURE 4. Breakdown times near the (1, 1, 1) mode resonance, $\theta = 5°, \omega = 2.640$.

It became clear during the initial experiments reported above, that the system being studied was extraordinarily rich in complex phenomena. A detailed mapping of even two dimensions of the ω–θ–E parameter space, listing breakdown regimes, would have been a formidable and time-consuming task. Given this situation, it was decided that only two modes were to be selected for study in detail: the fundamental or (1, 1, 1)-mode and the (3, 1, 1)-mode. The (1, 1, 1)-mode is an obvious choice as it is the lowest-order mode that can be forced in these experiments. The (3, 1, 1)-mode was selected as it is easily forced and its low number of axial wavelengths allows easy visualization of phenomena contributing to the breakdown. For these two modes it was interesting to investigate in detail a narrow bandwidth about the resonant frequency. Breakdown times were measured as a function of the parameters ω, θ and E for these small slices of parameter space. The interest was in determining the details of the breakdown behaviour where three modes were closely spaced in the ω-spectrum, namely the (1, 1, 1)-, (2, 2, 1)- and (3, 3, 1)-modes in the one case, and the (3, 1, 1)-, (6, 2, 1)- and (9, 3, 1)-modes in the other. Refer to table 1 to see the resonant ω for these modes. For these two modes, approximate limits to θ were found within which a breakdown did not occur in one of the specific regimes detailed shortly.

4.2.3. *Effect of boundary layers on the breakdown*

The Ekman layer thickness scales non-dimensionally as $E^{\frac{1}{2}}$ (Greenspan 1968). Experiments were conducted to determine the influence of boundary-layer thickness on the flow breakdown behaviour. It was found that the breakdown times are insensitive to $E^{\frac{1}{2}}$, from which it can be inferred that variations in boundary-layer thickness do not influence the breakdown behaviour. For the value of $\theta = 5°$ used in these experiments the form of the breakdown was also independent of E – it was the Type A breakdown detailed in §4.3.2. One cannot of course assume that viscosity is unimportant to the breakdown processes; some energy dissipation may result, for example, in the destabilizing wave–mean flow interactions discussed in §5.2.

For these experiments in which the Ekman number was varied, E was defined as $\nu/((\omega_1+\omega_2)L^2)$. Use of this standard definition ensured that the effect of the

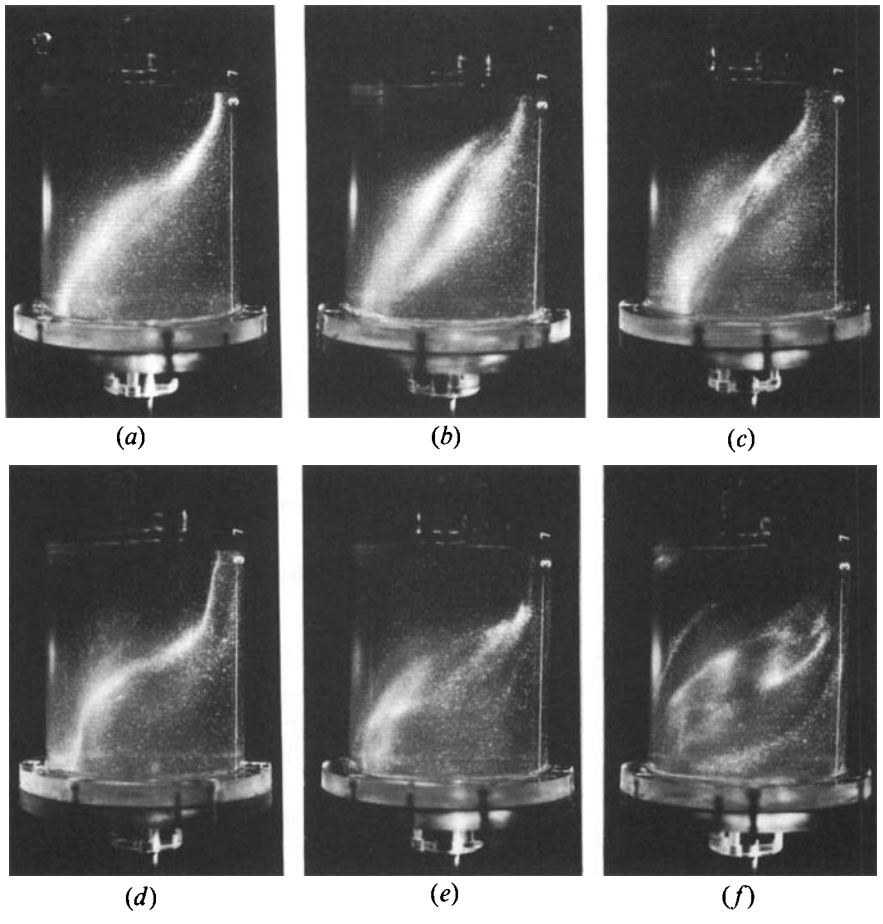

FIGURE 5(*a–f*). For caption see facing page.

precession on the boundary-layer thickness was included, an important factor in *retrograde* precession when $\omega_2 < 0$. The Ekman layer thickness $E^{\frac{1}{2}}$ is increased simply by operating at a lower ω_1 and ensuring that ω_2 is scaled to maintain a resonant ω. Figure 4 shows the variation of the breakdown time t_c with $E^{\frac{1}{2}}$ for breakdowns of the (1, 1, 1)-mode. Checks were also made for other modes and similar results were obtained. Note that unlike following plots describing the effect of parameters θ and ω, t_c has not been plotted logarithmically. The vertical bars indicate 90% statistical confidence limits. Repeated measurements, typically 10, were made both to determine the magnitude of any random errors in measurement, and to aid in the selection of an operating ω_1 with a minimum in variance due to error in timing the breakdowns. The chosen operating ω_1 for the rest of the experimental study was 100 r.p.m. (10.47 rad s^{-1}). Here this corresponds to $E^{\frac{1}{2}} = 3.0 \times 10^{-3}$; the lowest $E^{\frac{1}{2}}$ plotted represents 13.4 rad s^{-1}, and the highest represents 2.36 rad s^{-1}. A doubling of the viscous boundary layer produces only a marginal increase in breakdown time, while a reduction in boundary-layer thickness from the operating value seems to have little effect.

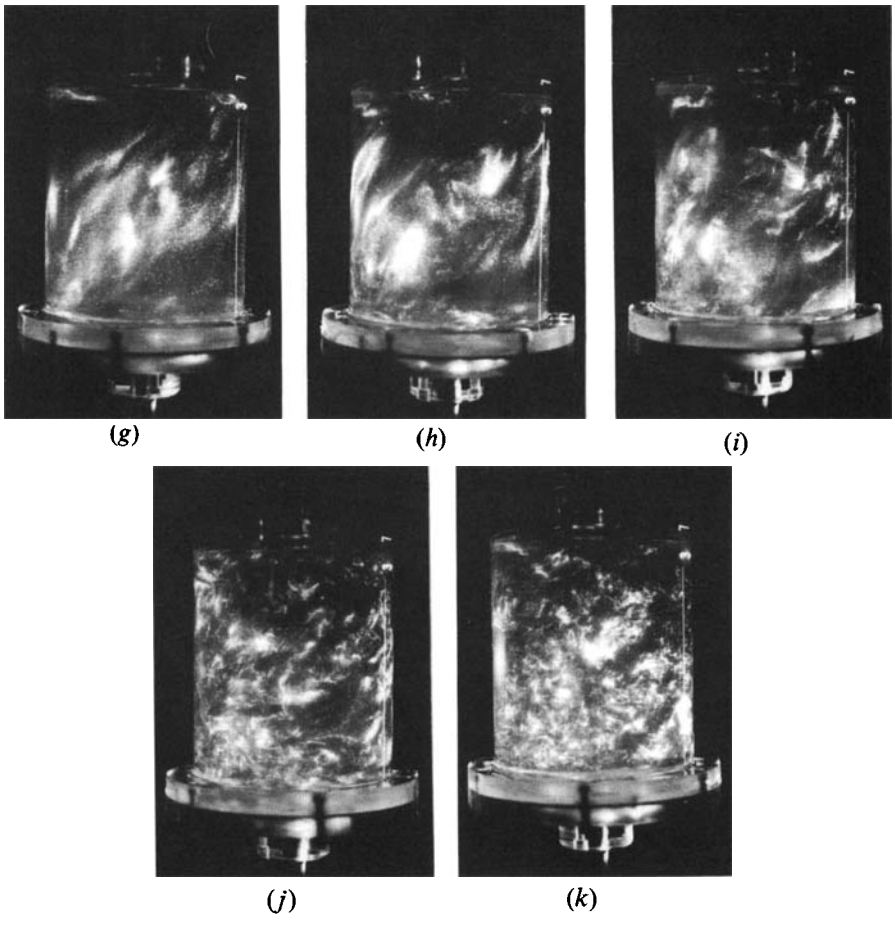

FIGURE 5. Type A breakdown, $\theta = 3°, \omega = 2.720$; (*a*) to (*k*) were taken at 0.3 s (0.5 revolution) intervals.

4.3. *Breakdowns of the* (1, 1, 1)*-mode*

4.3.1. *General*

This lowest-order or fundamental mode is the most easily forced, and exhibits the most dramatic breakdown behaviour. By the same token, it is harder to distinguish subtle variations in the behaviour of this mode, so it is in a sense less interesting than the (3, 1, 1)-mode described below. Effects of variations in both θ and ω were investigated. Precessional forcing was started by an impulsive tilt in the spin axis.

In the descriptions below of the pearlescent visualizations of both the (1, 1, 1)- and (3, 1, 1)-mode, the term *spatial extent* will be used to describe the apparent 'amplitude' of the bright pattern in the image of the tank. It should be remembered that in the majority of cases this has no correlation with the actual amplitude of the mode. The oscillatory flow due to the inertia waves is of sufficient magnitude to overwhelm the anomaly drift. As a consequence we see only the strain distribution corresponding to the inertia waves, which gives us a pattern independent of their amplitude.

Immediately on the impulsive tilt in spin axis, the core appears to incline rapidly, until it appears as almost a diagonal of the tank when viewed side-on. Figure 5(*a*)

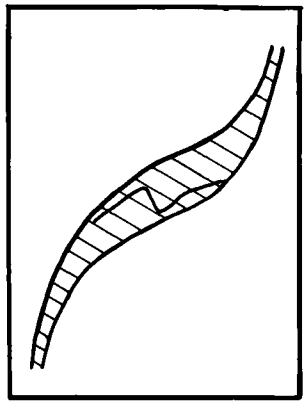

FIGURE 6. Sketch of stage (iii) in the Type A breakdown process. Solid lines indicate a temporally evolving but not oscillatory feature. Hatching indicates a luminous zone in the reflected pattern.

shows this case. This is interpreted as the rapid development of a modal flow with an axial structure that is a half sine wave, $\cos(\pi[z/h+\frac{1}{2}])$, for $-\frac{1}{2} < z/h < \frac{1}{2}$ as expected from (5).

Three major breakdown regimes are described below for this mode. The observations are related to the dynamic behaviour best illustrated by the playback of video recordings; however here they have been illustrated with still photographs. An attempt has been made to depict one stage in most of the breakdown processes with a sketch (figures 6 and 8). Although inevitably impressionistic, the sketches may compensate in part for the lack of a video playback. Refer to figure 10 to see the distribution of breakdown types in the θ–ω parameter space. Numerals below symbols indicate the number of multiple breakdowns (of the Type C, to be described shortly) recorded there.

4.3.2. *Type A breakdown*

This predominant breakdown regime, characterized by a rapid transition to fine-scale turbulence, occurs for all but the weakest forcing cases. Figure 5(*a–k*) shows the behaviour up to this type of breakdown. All the photographic exposures presented in this study took $\frac{1}{250}$ of a second. Here the exposures were made at 0.3 s or 0.5 revolution intervals. The frequency was $\omega = 2.72$ and the nutation angle $\theta = 3°$.

Figure 5(*a*) is a photograph taken about 3 revolutions after the impulsive tilt.

(i) The core waveform grows very rapidly in spatial extent and reaches a maximum in a few revolutions. Figure 5(*d*) shows the waveform at its maximum just prior to breakdown.

(ii) Interesting behaviour can be observed where the cylinder axis intersects the waveform, i.e. at the inflexion point of the sinusoidal wave. In some cases the luminous zone here appears to split into two filaments and then rejoin. Figures 5(*b*) and 5(*c*) show this occurring.

(iii) The region of the core around the inflexion point develops a modulation; a single superimposed wave of small wavelength. Just before the transition to turbulence, this modulated region develops to quite large local spatial extent. This dynamic behaviour is clearer on video than in still photographs; it occurs at the stages of figures 5(*f*) and 5(*g*), and is illustrated with a sketch (figure 6).

(iv) Fluctuations appear at the corners of the cylindrical section being viewed, at about the stage of figure 5(*g*), but almost instantly turbulence fills the whole tank. Within a couple of revolutions this turbulence has its smallest lengthscales, as shown

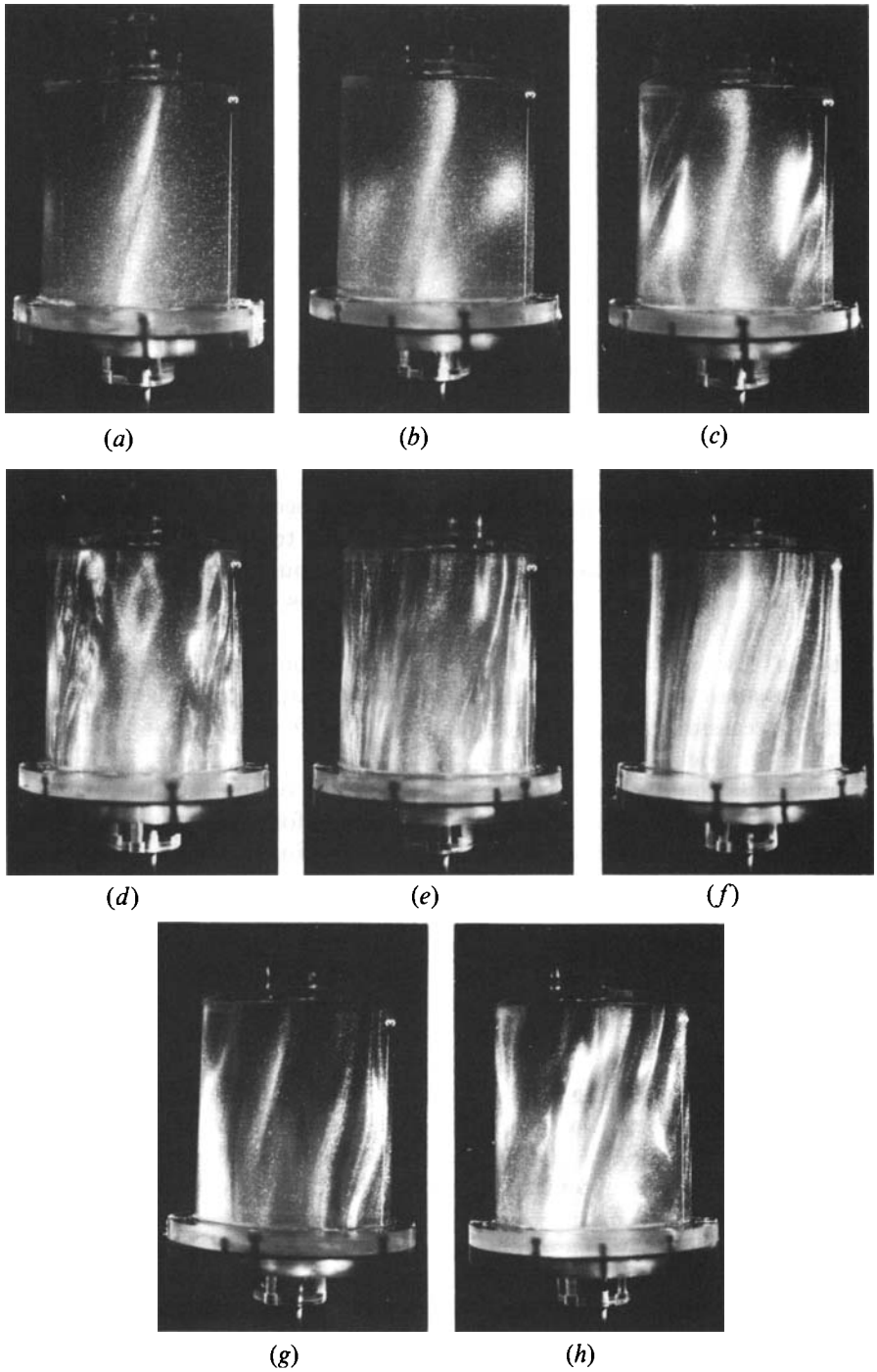

FIGURE 7. (*a–f*) Type B breakdown, $\theta = 0.4°, \omega = 2.635$, taken at irregular intervals due to the slower evolution of this regime. (*g*, *h*) Type C breakdown, $\theta = 0.4°, \omega = 2.635$; (*g*) and (*h*) follow (*a*) to (*f*) in time; however, they were taken about a minute (100 revolutions) after (*f*).

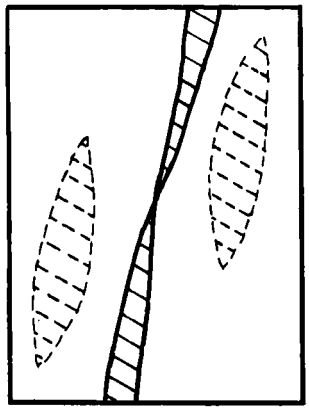

FIGURE 8. Sketch of stage (ii) in the Type B breakdown process. Solid lines indicate a temporally evolving but not oscillatory feature. Dashed lines indicate an oscillatory feature. Hatching indicates a luminous zone in the reflected pattern.

in figure 5(*k*). This climax to the breakdown process occurs at about 10 revolutions after the impulsive tilt. The breakdown time is judged to have elapsed by this point.

(v) Immediately on breakdown the highly turbulent flow shows a strong circulation when viewed in the precessing frame. This flow is counterclockwise on figure 5.

(vi) After a few more revolutions this circulation stops. The fluid remains turbulent with small isotropic lengthscales but there appears to be no bulk motion at all in the precessing frame. The circulation then re-establishes itself but in the reverse sense, i.e. clockwise on figure 5.

(vii) The circulation appears to cease. The annular region begins to pulsate with a frequency in the order of ω_1. This may happen before or during the circulation reversal. The turbulent zone bounded by the annulus inner radius forms an inclined core along the pattern of the original waveform. The pulsations wax and wane but the flow remains turbulent as long as the forcing is maintained.

The timescales quoted above are typical of Type A breakdowns occurring at $\theta = 3°$ or above. However, breakdowns best described as Type A can also occur over longer timescales, of about 50 revolutions, for $\theta = 1°$ and $\omega < 2.62$.

4.3.3. *Type B breakdown*

This occurs for weak forcing cases, does not result in fine-scale turbulence, and appears to involve a protracted interaction with another mode. A typical Type B breakdown is shown in figures 7(*a*)–7(*f*), which were not taken at regular intervals owing to the much slower evolution of this regime. The frequency was $\omega = 2.635$, which is just below the resonance, and the nutation angle $\theta = 0.4°$.

(i) As seen in figure 7(*a*), the growth in spatial extent of the waveform is slower and the core does not incline to the extent that it does for a Type A breakdown.

(ii) Some fluctuations can be discerned in the background body of the fluid. Rapidly fluctuating bright patches appear on either side of the inclined core, as in figure 7(*b*). This stage is illustrated with a sketch (figure 8).

(iii) The patches become better defined and some axial modality can be made out; approximately 1.5 wavelengths can be discerned during videotape playback.

(iv) Fine-scale disorder appears in the flow and the core waveform is obliterated. This occurs at about 30–40 revolutions after the impulsive tilt, in between figures 7(*d*) and 7(*e*).

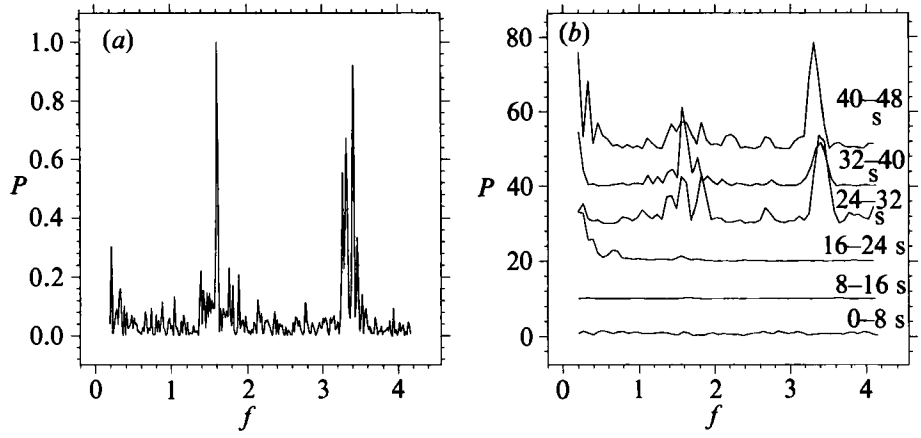

FIGURE 9. Type B breakdown, $\theta = 1°, \omega = 2.600$. Frequency spectrum in s^{-1} of the reflected light intensity at a point ($r = 0.25, z = 0.63$). The data used covered 48 s; the breakdown occurred at about 22 s. (*a*) Spectrum of the whole 48 s, normalized to its peak value; the values on the ordinate have no physical meaning in terms of fluid flow variables, but the location of the peaks identifies periodicities in the flow. (*b*) Segmented spectra, normalized to the square of the average intensity over the whole 48 s. As in (*a*), the values on the ordinate may be disregarded.

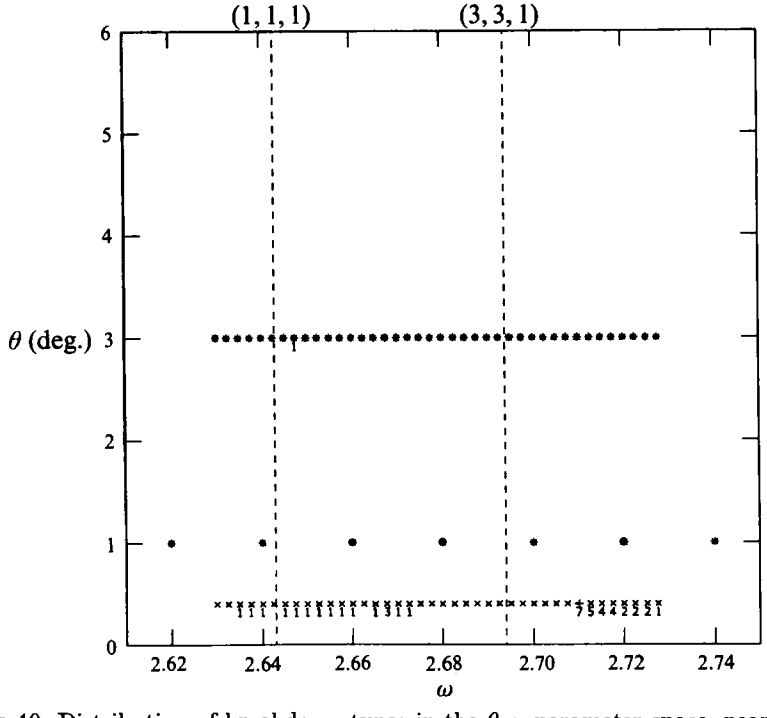

FIGURE 10. Distribution of breakdown types in the θ–ω parameter space, near the (1, 1, 1)-mode resonance, $E = 9 \times 10^{-6}$. *, Type A; ×, Type B; numerals below symbols indicate the number, if any, of multiple breakdowns (of Type C) occurring after a Type A or B breakdown. Vertical dashed lines indicate the location of low-order mode resonances.

(v) The fine scales in the disorder disappear in a few revolutions and the resulting flow is strongly columnar and inclined. Rapidly fluctuating inclined columns dominate the flow; however, it is hard to estimate the frequency of the fluctuations. In certain regions of parameter space, disorder never vanishes completely, but in

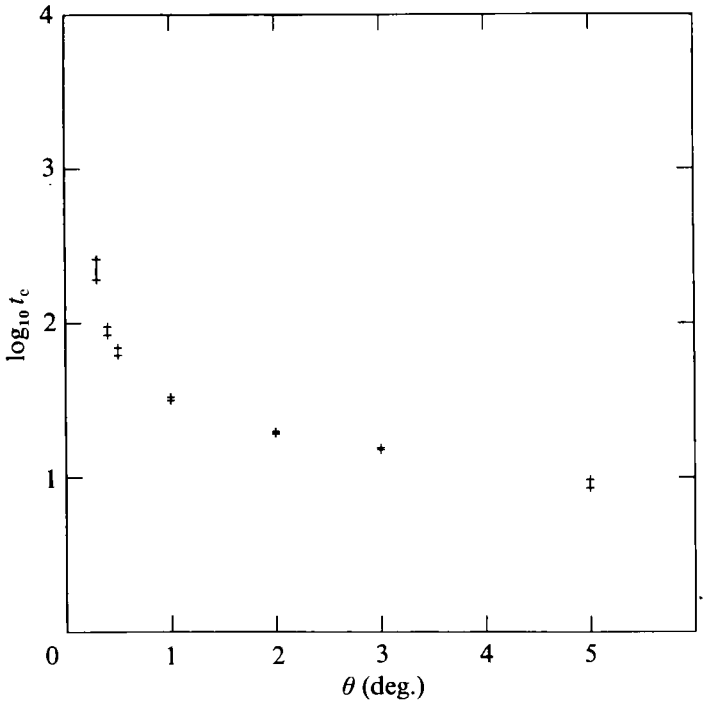

FIGURE 11. Breakdown times t_c (in revolutions) near the (1, 1, 1)-mode resonance, $\omega = 2.640$, $E = 9 \times 10^{-6}$. Vertical bars represent 90% statistical confidence limits. More than one breakdown type is included in this data.

others the flow becomes calm, as in figure 7(*f*), and one or more Type C breakdowns (detailed shortly) may follow.

In some other regions of parameter space, Type B breakdowns can also occur over longer timescales than those quoted here. For example at $\omega = 2.54$, which is further below the (1, 1, 1) mode resonance than the experiment in figure 7, and at $\theta = 1°$, Type B breakdowns occur at about 100 revolutions.

Figures 9(*a*) and 9(*b*) present data representing a Type B breakdown. Here the time dependence of the flow has been measured from the intensity of the light reflected by the pearlescent flakes. They were obtained by image processing of the video pictures, after a careful series of tests to ensure that any peaks in the spectra were due to features in the flow and not to spurious reflections of irregularities in the tank wall. The segmented spectra, normalized to the square of the average intensity recorded over the whole time series, show that the periodicities in the flow develop after the Type B breakdown. Recall that from the frame of reference in which the recordings were made, we should expect no time variation if the behaviour is consistent with a steady linear forced response. The peaks in the spectra give a quantification of the frequency of the 'rapidly fluctuating inclined columns' noted under point (v) above.

4.3.4. *Type C breakdown*

Type C breakdowns generally occur after a previous breakdown. Only one instance was noted where it occurred as the first breakdown. It is poorly defined; here it is illustrated with figures 7(*g*) and 7(*h*). It begins with increasing disorder in the corners of the cylindrical section in view. Disorder spreads throughout the tank, disrupting

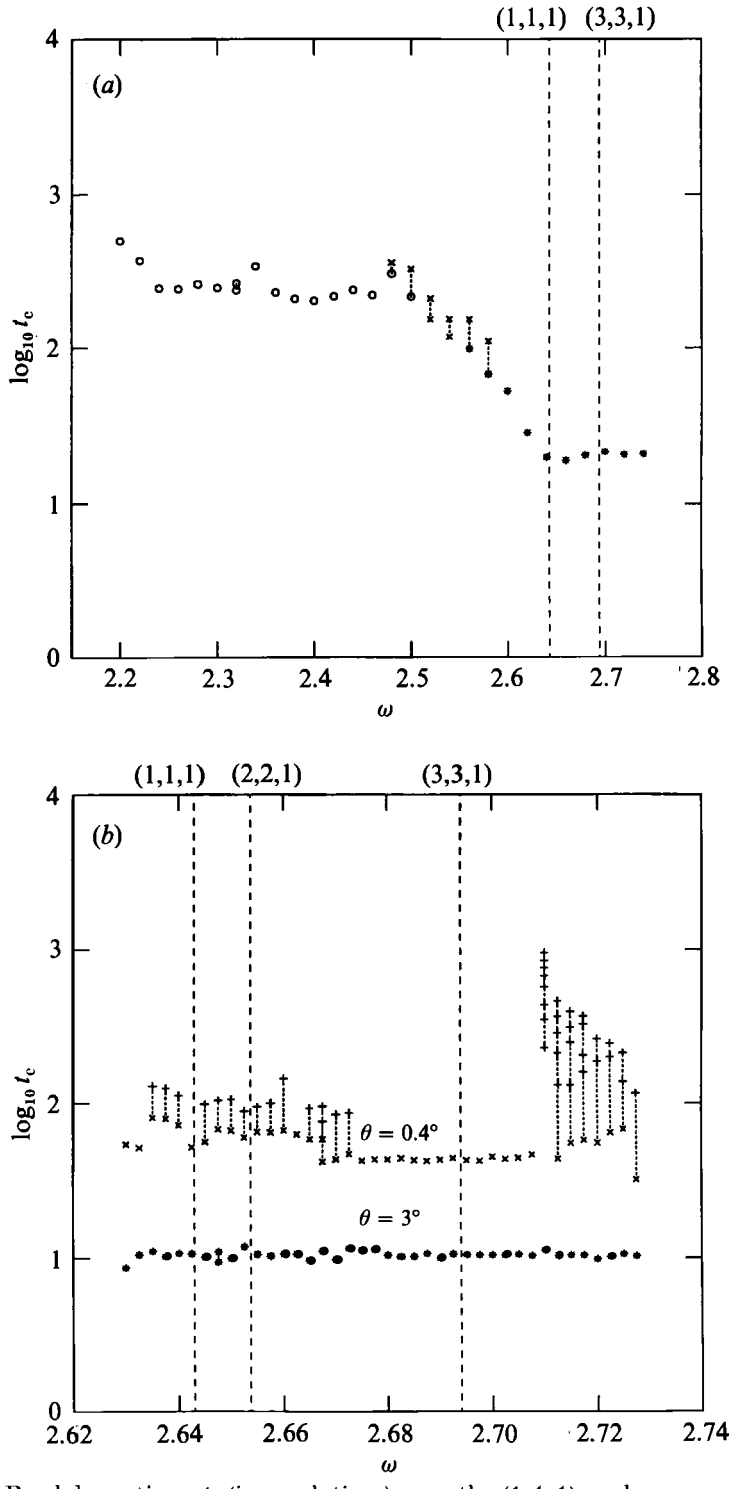

FIGURE 12. Breakdown times t_c (in revolutions) near the (1, 1, 1)-mode resonance, $E = 9 \times 10^{-6}$. Vertical dashed lines indicate the location of low-order mode resonances, vertical dotted lines connect multiple breakdowns. (*a*) $\theta = 1°$; *, Type A; ×, Type B; ○, long-timescale instabilities. (*b*) $\theta = 0.4°$ and $\theta = 3°$; *, Type A; ×, Type B; +, Type C.

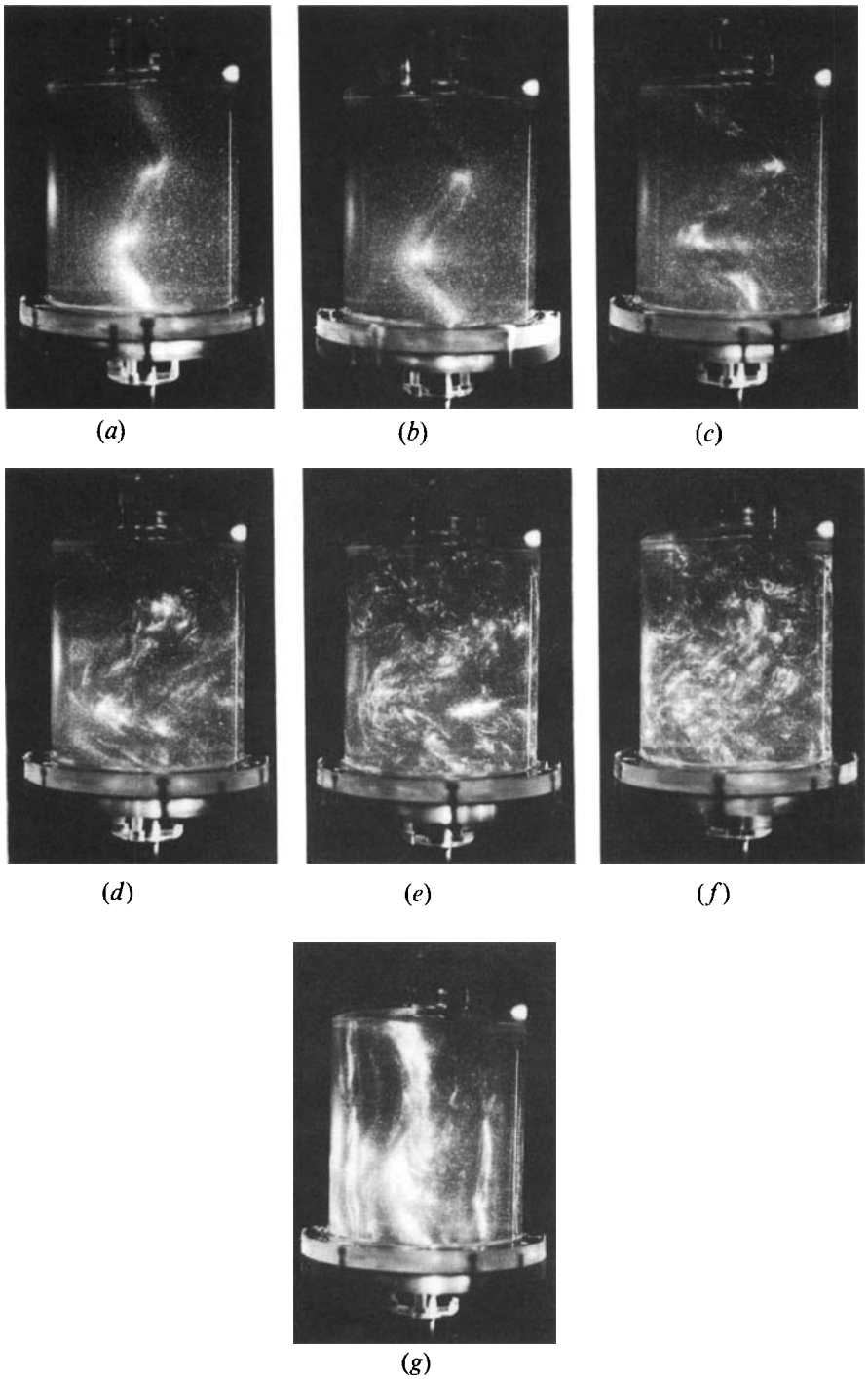

FIGURE 13(*a–g*). Type D breakdown, $\theta = 3°, \omega = 1.290$, not taken at regular intervals.

the columnar pattern established after the previous breakdown. In some cases the disorder wanes and the columnar pattern is re-established, leading to a further breakdown. Up to eight such consecutive Type C breakdowns have been observed; under these circumstances it appeared as though recurrent breakdowns would

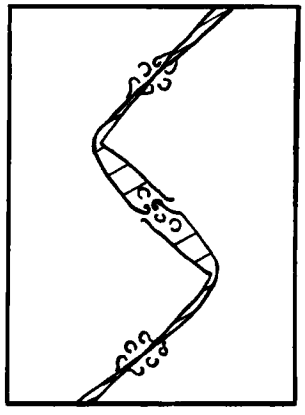

FIGURE 14. Sketch of stage (iii) in the Type D breakdown process. Solid lines indicate a temporally evolving but not oscillatory feature. Hatching indicates a luminous zone in the reflected pattern. Broken curved lines indicate turbulent features.

continue indefinitely. But in other cases the flow remains disordered after the first Type C breakdown.

4.3.5. *Variations in the θ–ω parameter space*

Figure 10 shows the distribution of breakdown types in θ–ω parameter space. Quantitative data for the time for the breakdowns to occur were also taken. Figure 11 summarizes the results for variations in θ, the tests being done at the (1, 1, 1)-mode resonant frequency. In figure 11 the data includes timings of different breakdown regimes. The breakdown timings were particularly consistent for this strong forcing case, so 90% statistical confidence intervals have been employed. (However, there are systematic shifts in the breakdown times between different sets of experiments. Evidence of this is the difference in the breakdown times for $\theta = 3°$ presented in figure 11 and figure 12(*b*). The differences are consistent with an unavoidable change in the zero-setting of the spin and precession axes made between these sets of experiments, that altered the way the forced flow was set up.) The limiting angle for θ is about 0.3°, for our operating E value of 9×10^{-6}, and some form of breakdown was observed for all $\theta \geqslant 0.3°$.

Figure 12(*a*) shows the results for $\theta = 1°$ over a wide bandwidth in the ω-spectrum. Different breakdown regimes are indicated, with * for Type A and × for Type B. The ○ symbols indicate a weak instability, characterized by general disorder with long lengthscales, occurring over a long timescale. Vertical dotted lines connect multiple breakdowns. The time to each breakdown is measured from the start, $t = 0$. Figure 12(*b*) shows the results for a smaller slice of the ω-spectrum where three modes are closely spaced. Here Type C breakdowns are denoted by +. Resonant ω for the three modes of interest are marked.

4.4. *Breakdowns of the* (3, 1, 1)*-mode*

4.4.1. *General*

Here a two-parameter space was again investigated: the effect of variations in θ and ω. Refer to the θ–ω parameter space regime diagram (figure 22). As with the (1, 1, 1)-mode, breakdown times vary greatly with the forcing parameter θ; however, more interesting differences in qualitative behaviour were observed as ω was varied. As before precessional forcing was started by an impulsive tilt in the spin axis.

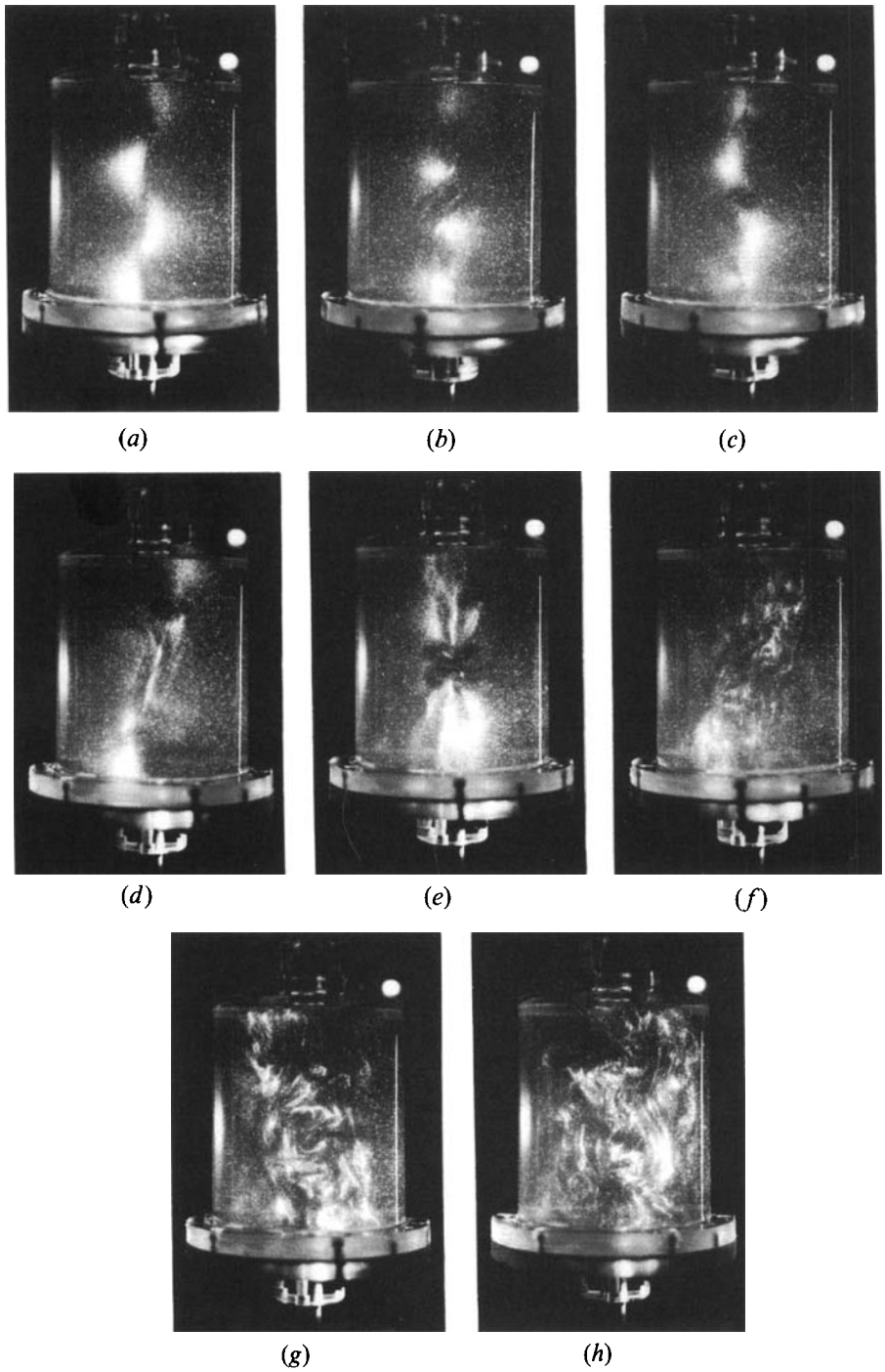

FIGURE 15(*a–h*). Type E breakdown, $\theta = 3°, \omega = 1.200$, not taken at regular intervals.

Perhaps because this mode is less easily forced than the (1, 1, 1)-mode, more complicated types of behaviour can be distinguished. Four major breakdown regimes are described below. Some parallels can be drawn with equivalent breakdown regimes of the (1, 1, 1)-mode. However, a different set of letters (D–G) is used here for

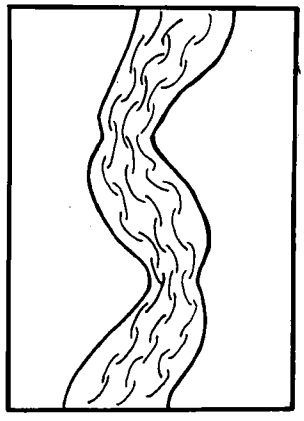

FIGURE 16. Sketch of stage (iv) in the Type E breakdown process. Solid lines indicate a temporally evolving but not oscillatory feature. Broken curved lines indicate turbulent features.

the breakdown types, to emphasize that behaviour regimes common to several modes may not exist. The quantitative measurements summarized in figures 20–22 will make clearer where in parameter space the different regimes occur for this mode. As with the Type A and B breakdowns of the (1, 1, 1)-mode, sketches (figures 14, 16, 18 and 19) have been made of a stage in each of the (3, 1, 1)-mode regimes detailed below.

4.4.2. *Type D breakdown*

This breakdown regime occurs in strong forcing cases and has the fastest breakdown times. Figures 13(*a*)–13(*g*) show its development. They were not taken at exactly spaced intervals but were cued off the video images in an attempt to illustrate important stages in the breakdown process. The frequency was $\omega = 1.29$ and the nutation angle $\theta = 3°$.

(i) The spatial extent of both the core and the luminous zone around it grow without waveform distortion (figure 13*a*, *b*).

(ii) At about five revolutions after the impulsive tilt, unsteadiness appears in the core (figure 13*c*); sometimes the luminous zone develops modulations of smaller wavelength.

(iii) Turbulence begins, apparently originating at each inflexion point of the sinusoidal wave. Recall that interesting phenomena were also noted at the inflexion point of the (1, 1, 1)-mode waveform. On close inspection of the region near the central inflexion point, the actual onset of turbulence can be discerned: the luminous zone appears to split into two filaments. In this sequence of photographs this has already occurred in figure 13(*a*). This stage is illustrated with a sketch (figure 14).

(iv) Fluctuations of higher frequencies rapidly dominate the general flow; turbulence spreads quickly outwards to the cylinder walls (figure 13*d*–*f*).

(v) Turbulence with small lengthscales is produced, as shown in figure 13(*f*). This is the climax of the breakdown process and the breakdown time is judged to be elapsed by this point. For strong forcing, this occurs at about 10 to 20 revolutions after the impulsive tilt.

(vi) The turbulence then becomes less fine-grain and by about 30 revolutions some order can once more be discerned in the flow. The modal waveform reappears superimposed on the general disorder, as in figure 13(*g*). However, the flow never completely recovers the ordered waveform present before breakdown.

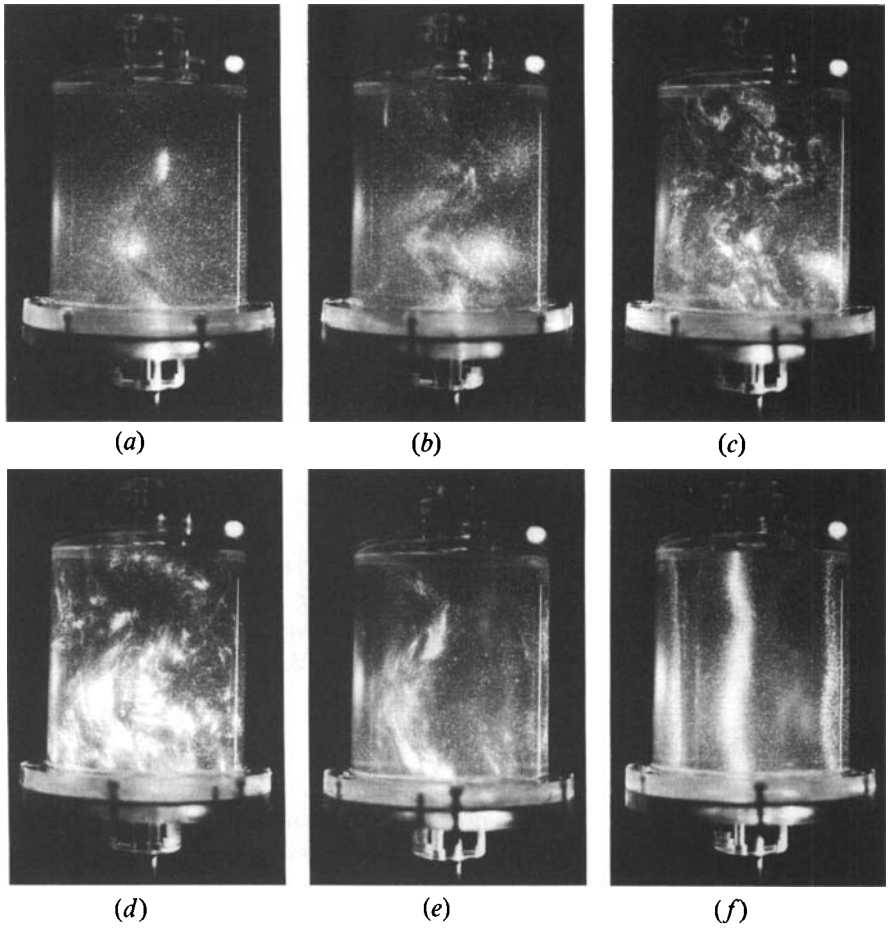

FIGURE 17(*a–f*). For caption see facing page.

4.4.3. *Type E breakdown*

This regime occurs for strong forcing nearer to the (3, 1, 1)-mode frequency than to the (6, 2, 1)-mode frequency. It is characterized by turbulence 'lingering' in the core region before spreading throughout the tank. Figures 15(*a*)–15(*h*) illustrate the process, once again not taken at regular intervals. Here they cover about 50 s. The frequency was $\omega = 1.20$ and the nutation angle $\theta = 3°$.

(i) The core spatial extent grows without waveform distortion, a stage already completed by figure 15(*a*).

(ii) At about five revolutions the spatial extent growth appears to halt; the luminous zone becomes concentrated into patches on the convex sides of the wave crests.

(iii) Turbulence begins, again apparently originating at the waveform inflexion points (figure 15*b*).

(iv) In figure 15(*c–e*) the core becomes disordered, and its spatial extent shrinks until the original waveform can no longer be discerned. Occasionally, higher axial wavenumbers can be made out. Although not captured in this sequence of photographs, the original waveform generally reappears and grows in spatial extent again. This stage is illustrated with a sketch (figure 16). A few cycles of this process can be made out over the next few revolutions, as:

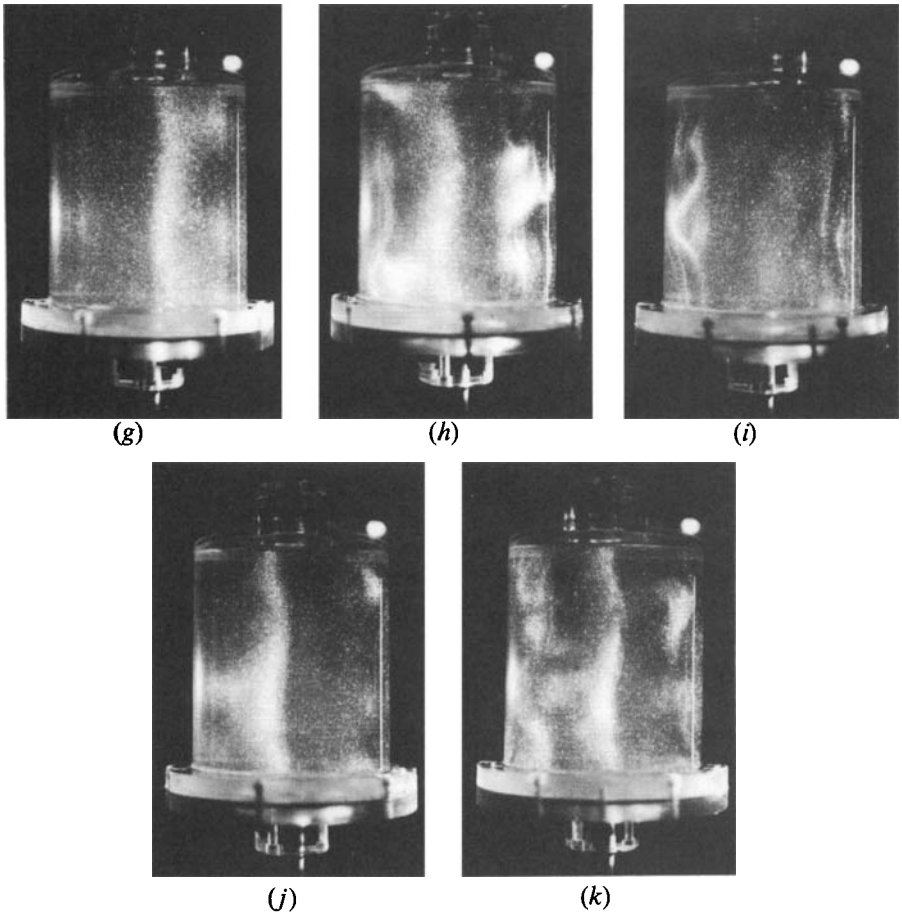

FIGURE 17. (*a–f*) Type F breakdown, $\theta = 1°, \omega = 1.260$, taken at approximately 2 s intervals. (*g–k*) Type G breakdown, $\theta = 1°, \omega = 1.260$. (*g–k*) follow (*a–f*) in time; however, they were not taken at regular intervals.

(v) the disordered core gradually enlarges until it reaches the cylinder walls (figure 15*f–h*). As it nears the walls, high-frequency fluctuations can be noted in an annulus between the core and the walls.

(vi) The breakdown reaches its climax as the turbulence attains its smallest eddy size, when the breakdown time is judged to have elapsed. This occurs at about 30 revolutions, and in this sequence is just after figure 15(*h*). As in the Type D breakdown, a modal ordering of the flow is soon recovered as the turbulence lengthscales become larger. However, the subsequent flow is never free of disorder.

4.4.4. *Type F breakdown*

This regime occurs for weaker forcing nearer to the (3, 1, 1)-mode frequency than to the (6, 2, 1)-mode frequency. Figures 17(*a*)–17(*f*) show the development of this type of breakdown. They were taken at approximately 2 s intervals. The frequency was $\omega = 1.260$ and the nutation angle $\theta = 1°$.

(i) In figure 17(*a*), the core and luminous zone spatial extent grow slowly and not necessarily monotonically. Sometimes the spatial extent shrinks and then grows again.

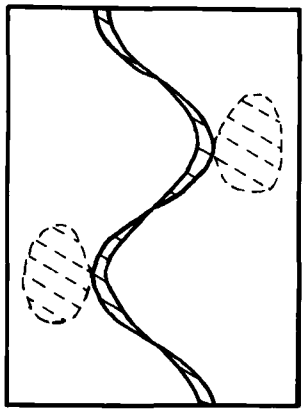

FIGURE 18. Sketch of stage (ii) in the Type F breakdown process. Solid lines indicate a temporally evolving but not oscillatory feature. Dashed lines indicate an oscillatory feature. Hatching indicates a luminous zone in the reflected pattern.

(ii) Luminous regions extend from the convex sides of the wave crests into the body of the fluid. This stage falls in between figures 17 (*a*) and 17 (*b*), and is illustrated with a sketch (figure 18).

(iii) Instability in the core appears at about 30 revolutions, at the waveform inflexion points.

(iv) Oscillating bright patches appear, extending from the core into the fluid body. This stage is almost completed in figure 17 (*b*).

(v) In figures 17 (*c*) and 17 (*d*) the core waveform becomes distorted, and almost simultaneously disorder rapidly fills the whole tank. At this point the breakdown time is judged to have elapsed.

(vi) The flow becomes more ordered though still unsteady: a wavy bright column can be seen, apparently rotating with the tank, as shown in figure 17 (*f*). The number of axial wavelengths is clearly 1.5 at times, and approximately 3 at others. In certain regions of the forcing frequency spectrum a series of Type G breakdowns (detailed below) will follow.

4.4.5. *Type G breakdown*

This occurs as a secondary breakdown after a Type F breakdown, or occasionally by itself at a frequency nearer the (6, 2, 1)- or (9, 3, 1)-mode frequencies. Here this type of breakdown is illustrated by figures 17 (*g*)–17 (*k*) which are part of the same sequence as figures 17 (*a*)–17 (*f*). However, figures 17 (*g*)–17 (*k*) were not taken at regular intervals; they are spaced out over about 2 minutes.

(i) For a period of time corresponding to about 100 revolutions, the flow is basically ordered, consisting of a wavy bright column as above. Gradually, fluctuations in brightness can be discerned along the vertical cylinder walls, as in figure 17 (*g*), confined to an annular region of width less than about $\frac{1}{2}r$. This behaviour appears very similar to a Type B breakdown of the (1, 1, 1)-mode.

(ii) The fluctuations in the annular region become better defined until some axial modality can be made out. There appear to be either 3 axial wavelengths or superimposed waveforms of 1.5 wavelengths. This occurs between figures 17 (*h*) and 17 (*i*), and is illustrated with a sketch (figure 19).

(iii) In figure 17 (*i*) sharper but unsteady patterns, apparently consisting of

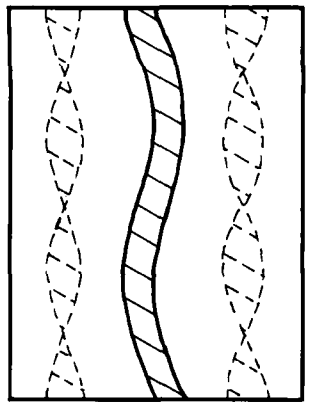

FIGURE 19. Sketch of stage (ii) in the Type G breakdown process. Solid lines indicate a temporally evolving but not oscillatory feature. Dashed lines indicate an oscillatory feature. Hatching indicates a luminous zone in the reflected pattern.

intertwined waveforms of 1.5 axial wavelengths, grow inwards, destabilizing the core. The whole flow becomes disordered, at about 200 to 300 revolutions after the initial breakdown.

(iv) Turbulent eddies are never created. The patterns remain strongly columnar and soon a state similar to the one before breakdown is recovered, as in figure 17(*j*).

(v) The breakdown process will repeat itself. Times were recorded for up to seven Type G breakdowns in sequence; a period in the order of 100 revolutions separates each breakdown. The beginnings of a second Type G breakdown is shown in figure 17(*k*).

In some cases, the later breakdowns were less distinct, and eventually appeared to be subsumed in the general disorder. However, in other cases this rough cycling was sustained as if it would continue indefinitely, a series of chaotic bursts being separated by long periods of order. It may have been that this sustained intermittency was systematically located in certain regions of parameter space, and that the cases where recurring breakdowns died out were located in others. Alternatively, random experimental inaccuracies may have engendered the demise of sustained intermittency in some of the runs. It may be that a more accurate apparatus with temperature control is required for a proper investigation of this phenomenon.

4.4.6. *Variations in the θ–ω parameter space*

Figure 20 summarizes the results of variations in the forcing parameter θ. Some regimes shown on this figure were not described in detail above but will be noted below. The tests were done near the (3, 1, 1)-mode resonant frequency. The limiting value in θ is about 0.8°, at our operating value of $E = 9.0 \times 10^{-6}$. For θ less than 0.8° breakdowns of the types detailed above were not noted and the modal waveform can still be observed. Its spatial extent is small and does not appear to change. Clearly Type D breakdowns are favoured when the forcing is strongest, and Type F breakdowns at weak forcing. However, there is overlap of the breakdown regimes. As noted in §4.2.2, it is not clear whether small variations in the initial conditions or different running conditions cause one particular regime to be selected over another for an otherwise identical experimental run.

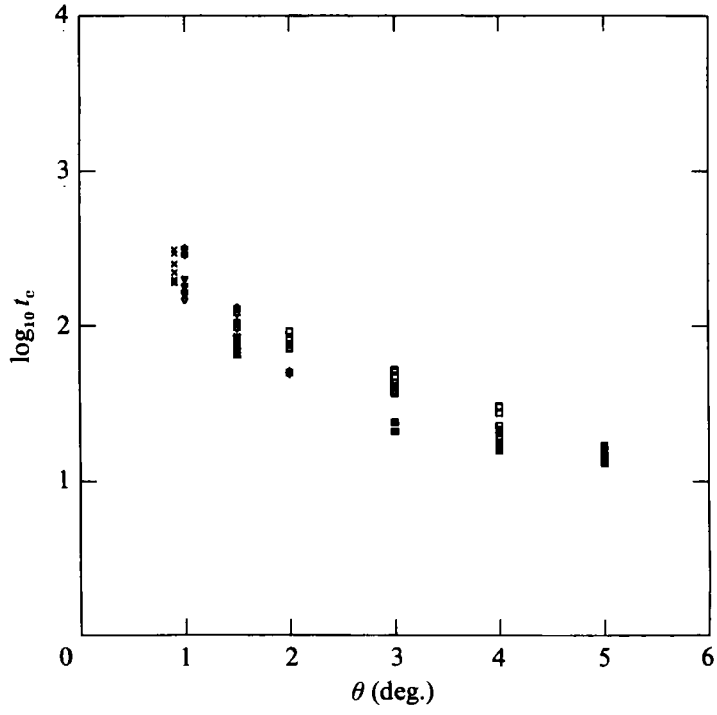

FIGURE 20. Breakdown times t_c (in revolutions) near the (3, 1, 1)-mode resonance, $\omega = 1.224$, $E = 9 \times 10^{-6}$: ⊠, Type D; □, Type E; ☆, Type F; △, Type F1; ▽, Type F2; ×, Type G.

Figure 21 (*a–c*) summarizes the results of variations in the forcing frequency ω, for the narrow bandwidth of interest around the linear resonant frequency. Where ○ symbols occur on the abscissa, only long-timescale instabilities (of the form described in §4.1) occurring after about 1000 revolutions were noted. Once again different breakdown regimes are evident: Type F breakdowns are prevalent for weaker forcing cases and Type D breakdowns for stronger forcing cases. It is important to note that while a pure Type D breakdown is readily distinguished from, say, a Type E breakdown, intermediate breakdown types do exist. For example, results for $\theta = 1°$ show a regime, Type F1, that has aspects of Type E behaviour. The results for $\theta = 1.5°$ show a regime, Type F2, with aspects of Type D behaviour. Some intermediate breakdown types appear to be restricted to small neighbouring regions of parameter space and may represent distinct sub-regimes. For example, only Type F and F2 breakdowns occurred in the experiments at $\theta = 1°$ and $\omega = 1.2236$ presented in figure 20, whereas slightly further away in frequency, Type F1 breakdowns were found, as shown on figure 21 (*a*), which represents the results of an independent set of experiments. It should be emphasized that apparently scattered points in the sort of data presented here do represent qualitatively different flows.

When the system is forced near to the resonant frequency of the (6, 2, 1)-mode, which is non-expressed, the mode visible is still the (3, 1, 1)-mode, which is dominant over this ω-bandwidth. Note that the bandwidths where a particular breakdown regime occurs are not centred on the (3, 1, 1)-mode resonance. In figure 22 the occurrence of each (3, 1, 1)-mode breakdown type is summarized in a regime diagram in θ–ω parameter space. Numerals below symbols indicate the number of multiple (Type G) breakdowns recorded here.

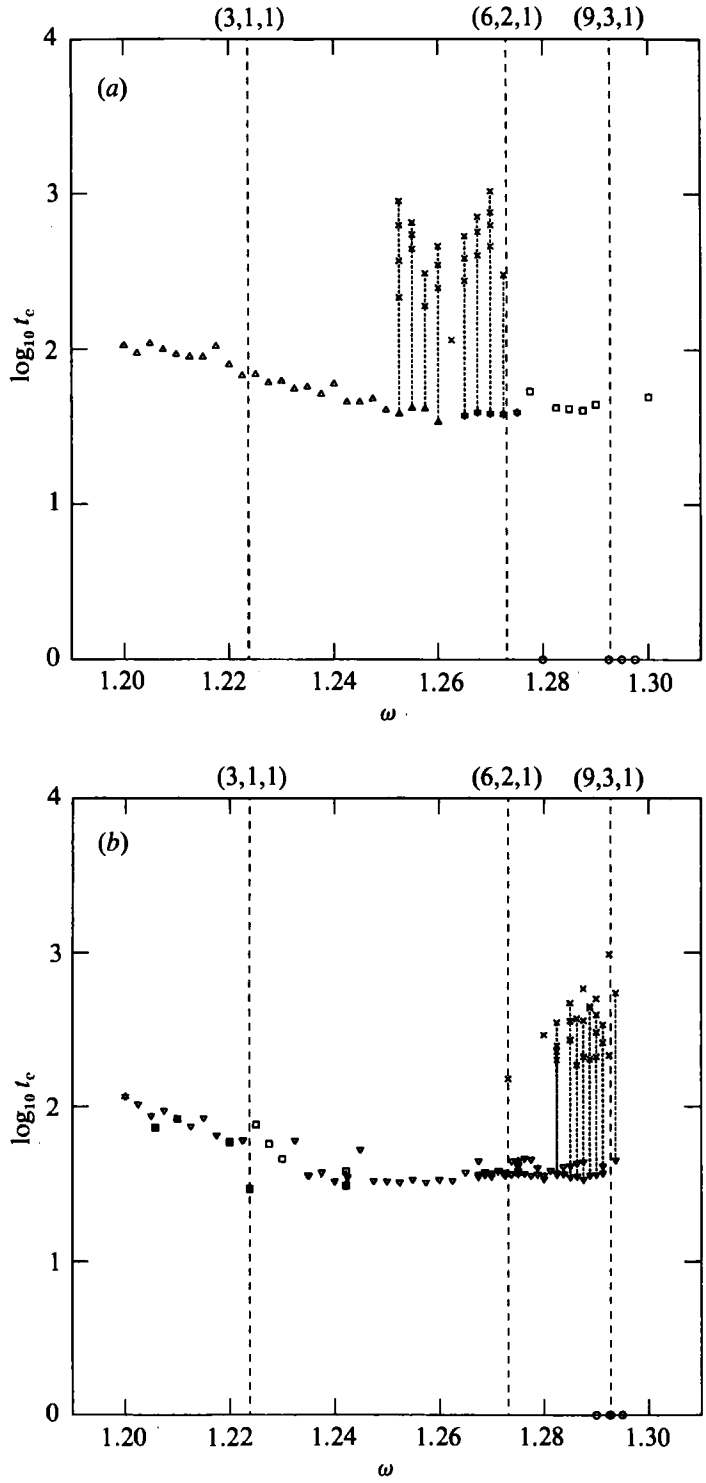

FIGURE 21 (*a–b*). For caption see facing page.

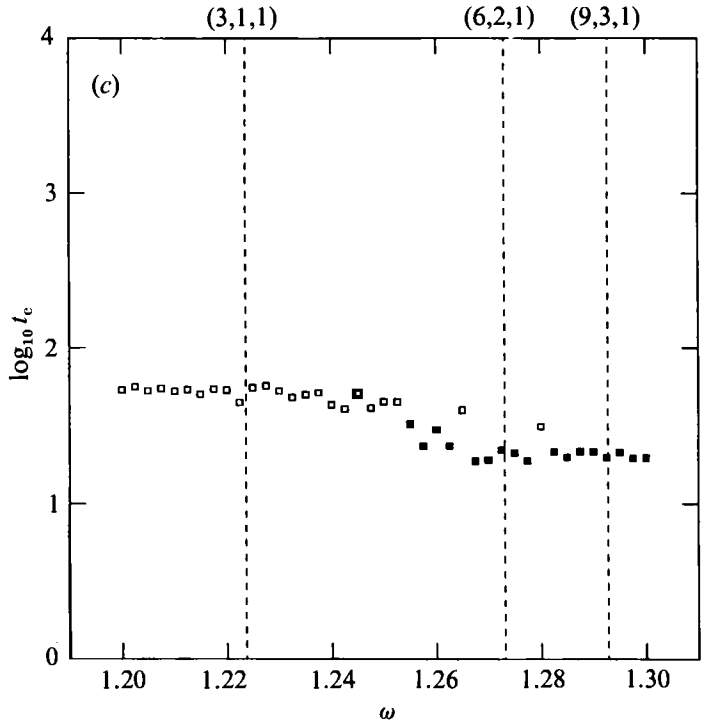

FIGURE 21. Breakdown times t_c (in revolutions) near the (3, 1, 1)-mode resonance, $E = 9 \times 10^{-6}$: symbols as figure 20, and ○, long-timescale instabilities. Vertical dashed lines indicate the location of low-order mode resonances. Vertical dotted lines connect multiple breakdowns. (*a*) $\theta = 1°$, (*b*) $\theta = 1.5°$, (*c*) $\theta = 3°$.

5. Discussion and conclusions

5.1. *Summary of the experimental observations*

This paper describes the first detailed observations of the fluid motion within a precessing cylinder. We identified patterns consistent with the presence of those low-order modes that one might reasonably expect to see evidence of with the apparatus used in these experiments, at approximately the frequencies predicted by linear inviscid theory. This should be considered as a substantial confirmation of the ability of linear inviscid theory to predict the resonant frequencies of low-order modes. The observations show that our system is extraordinarily rich, exhibiting, for example, intermittent breakdowns. The two modes studied in detail undergo a variety of breakdowns, ranging from the Type A and D breakdowns that we could call *violent collapses* to long-timescale instabilities. It was shown that variations in the Ekman number have little influence on the Type A breakdown, and that breakdowns in general take longer to occur for weaker forcing. In some of the regimes reported in §4, notably the Type B, C, F and G breakdowns, it appeared as though one or two secondary modes were interacting with the primary. The Type C and G breakdowns were notable by their intermittent behaviour.

A future paper will present the results of dyeline experiments. These later experiments provided further confirmation that linear inviscid theory can be used to predict the resonant frequencies of low-order inertia wave modes. Furthermore, some additional features of linear inviscid theory, in particular the oscillatory time dependence and the amplitude, seem initially to be in fair agreement with these

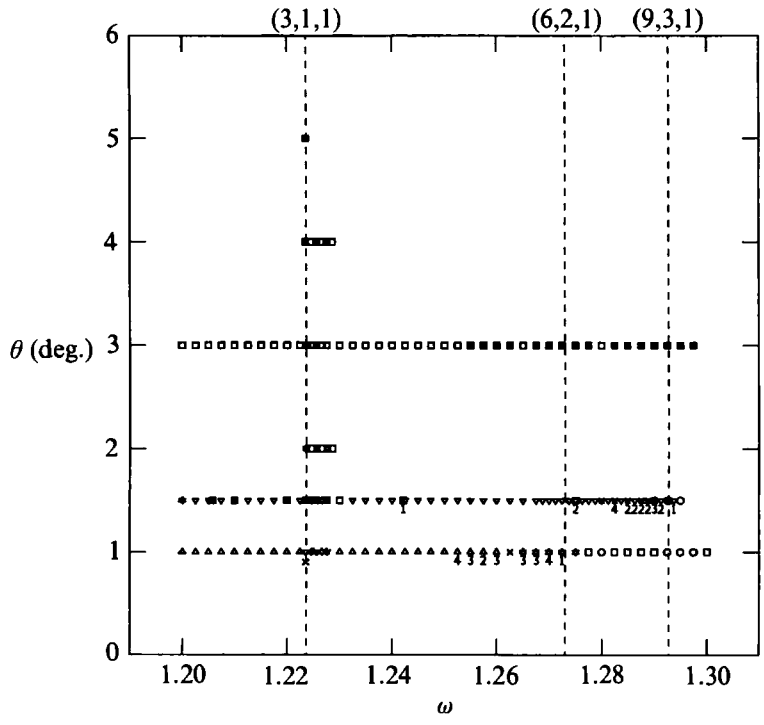

FIGURE 22. Distribution of breakdown types in the θ–ω parameter space, near the (3, 1, 1)-mode resonance, $E = 9 \times 10^{-6}$: symbols as figure 21. Numerals below symbols indicate the number, if any, of multiple breakdowns (of Type G) occurring after a breakdown. Some isolated first breakdowns occur that are also best described as Type G. Vertical dashed lines indicate the location of low-order mode resonances.

experiments. However, the dyeline experiments also indicated that departures from linear inviscid theory occur earlier than suspected from the pearlescence visualizations of the flow, and that for weak forcing away from low-order mode resonances, it is difficult to obtain much correspondence, even at early times, with linear inviscid theory.

5.2. *Some speculations*

Some authors have associated the 'resonant collapse' with a mean circulation. Gunn & Aldridge (1990) have made a theoretical study of the changes in the eigenfrequency spectrum due to a non-uniform rotation. They associated collapse with a sudden reduction in amplitude that would occur if a mean flow 'Doppler-shifted' the frequency away from resonance. However, it is not clear how this sort of *parametric* reduction in the amplitude of a mode corresponds to the *dynamic* breakdowns of inertia waves that have been observed by McEwan (1970), by Stergiopoulos & Aldridge (1982) in earlier experiments and as reported here in §4. Furthermore, in §4 it was noted that Type A breakdowns occur both near to (within 0.2% of) and well away from (within 5% of) the primary-mode resonant peak. These breakdowns were similar, both qualitatively and quantitatively, in terms of timescale to the breakdown. The proposed frequency shift does not account for all these observations, since well away from the primary-mode resonant peak, the small shift in frequency proposed would not correspond to the large reduction in amplitude that they associate with collapse. Gunn & Aldridge state that their frequency shift does not

account for the observed return to resonance in their experiments, which may be similar to the intermittency reported by McEwan (1970) and here in §4.

McEwan (1970) could show how an azimuthal circulation would arise, due to the torque exerted by the sloping top lid in his experiment. He made a heuristic analysis with the aim of identifying the main physical processes involved in the evolution of the flow before collapse. Nonlinear evolution equations were derived for the variation of the resonant-mode amplitude and an azimuthal circulation with time, which when integrated gave fair agreement for the time to peak amplitude. The evolution equations, however, could not model the collapse itself. We cannot adopt exactly the same procedure in our precessing tank as there is no net couple acting on a sloping top. We should nevertheless expect a net circulation as derived formally by Thompson (1970). This is driven by nonlinear interaction in the boundary layer and is small, of $O(\theta^2)$ in our case. Thus in our case the circulation generated by this mechanism is of order 10^{-4}, too small to cause a 'resonant collapse' as suggested by Gunn & Aldridge (1990).

The intermittent behaviour is suggestive of a transfer of energy from the basic rotation to the oscillatory behaviour, which builds in amplitude until a Type C or G breakdown occurs. The defect in the basic rotation would then appear as a mean flow. Then there would be a period of order 100 revolutions, when we presume viscous effects are restoring the basic rotation to its original value before the next breakdown. This is a concept which is attractive in its simplicity, that is believed to underlie similar phenomena, for example that reported in the paper by Griffiths & Linden (1985) on diffusion-driven motions in a rotating fluid. The timescale observed for the intermittencies is consistent with that based on Ekman-layer dissipation. However, we still lack a rigorous theoretical explanation for the transfer of a sufficiently large proportion of the oscillatory energy to and from a mean flow, that could explain the violent collapse.

McEwan (1971) speculated that, as with the degeneration of internal waves in a stratified fluid, the 'resonant collapse' of inertia wave modes was caused by nonlinear interactions of triads of waves. In this *resonant triad* mechanism, the quadratic nonlinear terms combine two modes to force a third; energy supplied to a low-order 'primary' mode can flow to a pair of 'parasitic' secondary modes and so on in a cascade to turbulence. As the wave modes in a rectilinear tank or in the ocean are simple Fourier modes the appropriate nonlinear evolution equations can be inferred *a posteriori* by equating those terms that satisfy the resonant triad condition. However, in our case the Bessel functions which make up one of the separated spatial eigenfunctions do not obey simple addition theorems as trigonometric functions do. Thus the wavenumbers in the radial direction need not sum to permit nonlinear interaction, and there appears to be no *a priori* method of inferring which groups of modes are important in any weakly nonlinear interaction. The author has made some numerical calculations that try to map out the sets of modes that interact with a given primary. It is anticipated that this work will be reported in the future.

5.3. *Concluding remarks*

In 1970 McEwan produced a thorough experimental paper. The two most important conclusions were that linear inviscid theory accurately predicts the frequencies at which low-order inertia wave modes resonate, but that this same approximation will ultimately fail in situations of practical interest.

One situation of practical engineering interest, which pertains to the stability of spinning spacecraft containing liquid fuels, leads to Ekman numbers of order 10^{-6}

and nutation angles that grow to greater than 10°. From the results presented here, it appears that in this parameter range an assumption that the flow remains linear would be incorrect. In this paper, therefore, there is a confirmation of these two conclusions presented by McEwan 22 years ago. There is also a confirmation of his observation of the repeatability of the violent-collapse process. In addition, a detailed description has been made of some of the ways in which contained inertia waves can break down. The variety of phenomena described in §4 suggests that no single mechanism will account for all the ways in which contained inertia waves can break down. Some of the breakdown regimes can probably be adequately described by a low number of modes, interacting in a weakly nonlinear way. However, an elucidation of the intensely nonlinear violent collapses appears to offer us an entirely new theoretical and experimental challenge.

Finally we should recall the observation (Malkus 1989) that two-dimensional elliptical flows can give rise to inertia wave modes which then undergo breakdowns that are qualitatively very similar to the violent collapses described here. This indicates that an understanding of the violent collapse may have a much wider applicability than to the simple experimental system described here.

This work was done while the author was a graduate student at the University of Cambridge, Department of Applied Mathematics and Theoretical Physics (DAMTP). I should like to thank my supervisor, Dr Paul F. Linden, for his continuing support and encouragement during this time. The work was part of a project sponsored by the British National Space Centre/Royal Aerospace Establishment, whose support is gratefully acknowledged. I should like to thank my other colleagues working on the project, Drs Michael E. McIntyre, David G. H. Tan and John C. Jackson, for many interesting and insightful discussions. The apparatus could not have been constructed without the skills of DAMTP technicians. I am grateful to Dr John Simpson for help with photography, Dr Stuart B. Dalziel for help with microcomputer interfacing and to Knud Lunde, who gave the manuscript a thorough reading.

REFERENCES

BAINES, P. G. 1967 Forced oscillations of an enclosed rotating fluid. *J. Fluid Mech.* **30**, 533–546.

FULTZ, D. 1959 A note on overstability, and the elastoid-inertia oscillations of Kelvin, Solberg and Bjerknes. *J. Met.* **16**, 199–208.

GANS, R. F. 1970 On the precession of a resonant cylinder. *J. Fluid Mech.* **41**, 865–872.

GLEDZER, YE. B., DOLZHANSKII, F. V. & OBOUKHOV, A. M. 1989 Instability of elliptical rotation and simple models of vortex fluid shows. *Abstracts, Euromech 245: The Effect of Background Rotation on Fluid Motions, Department of Applied Mathematics and Theoretical Physics, Cambridge, UK, April 10–13 1989.*

GLEDZER, YE. B., KOVIKOV, YU. V., OBOUKHOV, A. M. & CHUSOV, M. A. 1974 An investigation of the stability of liquid flows in a three-axis ellipsoid. *Izv. Acad. Sci. USSR Atmos. Ocean Phys. Bull.* **10** (2), 115–118.

GREENSPAN, H. P. 1968 *The Theory of Rotating Fluids.* Cambridge University Press.

GRIFFITHS, R. W. & LINDEN, P. F. 1985 Intermittent baroclinic instability and fluctuations in geophysical contexts. *Nature* **316**, 801–803.

GUNN, J. S. & ALDRIDGE, K. D. 1990 Inertial wave eigenfrequencies for a non-uniformly rotating fluid. *Phys. Fluids* A **2**, 2055–2060.

JOHNSON, L. E. 1967 The precessing cylinder. In *Notes on the 1967 Summer Study Program in Geophysical Fluid Dynamics at the Woods Hole Oceanographic Inst.* Ref. 67-54, pp. 85–108.

KELVIN, LORD 1880 Vibrations of a columnar vortex. *Phil. Mag.* **10**, 155–168.

KUDLICK, M. 1966 On transient motions in a contained rotating fluid. Ph.D. thesis, Massachusetts Institute of Technology, February 1966.

MALKUS, W. V. R. 1968 Precession of the Earth as the cause of geomagnetism. *Science* **160**, 259–264.

MALKUS, W. V. R. 1989 An experimental study of the global instabilities due to the tidal (elliptical) distortion of a rotating elastic cylinder. *Geophys. Astrophys. Fluid Dyn.* **48**, 123–134.

MANASSEH, R. 1991 Inertia wave breakdown: experiments in a precessing cylinder. Ph.D. thesis, University of Cambridge.

MCEWAN, A. D. 1970 Inertial oscillations in a rotating fluid cylinder. *J. Fluid Mech.* **40**, 603–640.

MCEWAN, A. D. 1971 Degeneration of resonantly-excited standing internal gravity waves. *J. Fluid Mech.* **50**, 431–448.

MCEWAN, A. D. 1983 Internal mixing in stratified fluids. *J. Fluid Mech.* **128**, 59–80.

MCEWAN, A. D., MANDER, D. W. & SMITH, R. K. 1972 Forced resonant second-order interaction between damped internal waves. *J. Fluid Mech.* **55**, 589–608.

SAVAŞ, Ö. 1985 On flow visualisation using reflective flakes. *J. Fluid Mech.* **152**, 235–248.

SCOTT, W. E. 1975 The frequency of inertial waves in a rotating, sectored cylinder. *J. Appl. Mech. Trans. ASME* E: **43**, 571–574.

STERGIOPOULOS, S. & ALDRIDGE, K. D. 1982 Inertial waves in a fluid partially filling a cylindrical cavity during spin-up from rest. *Geophys. Astrophys. Fluid Dyn.* **21**, 89–112.

SUESS, S. T. 1971 Viscous flow in a deformable rotating container. *J. Fluid Mech.* **45**, 189–201.

THOMPSON, R. 1970 Diurnal tides and shear instabilities in a rotating cylinder. *J. Fluid Mech.* **40**, 737–751.

WALEFFE, F. 1988 3D Instability of bounded elliptical flow. (*M.I.T.*) *Woods Hole GFD Fellow Report, August 1988.*

WHITING, R. D. 1981 An experimental study of forced asymmetric oscillations in a rotating liquid filled cylinder. *Ballistic Research Labs. Rep.* ARBRL-TR-02376.

WOOD, W. W. 1965 Properties of inviscid, recirculating flows. *J. Fluid Mech.* **22**, 337–346.

WOOD, W. W. 1966 An oscillatory disturbance of rigidly rotating fluid. *Proc. R. Soc. Lond.* A **293**, 181–212.